

# Measurement of the $\Lambda_b^0$ Decay Form Factor

DELPHI Collaboration

## Abstract

The form factor of  $\Lambda_b^0$  baryons is estimated using  $3.46 \cdot 10^6$  hadronic  $Z$  decays collected by the DELPHI experiment between 1992 and 1995. Charmed  $\Lambda_c^+$  baryons fully reconstructed in the  $pK^-\pi^+$ ,  $pK_S^0$ , and  $\Lambda\pi^+\pi^+\pi^-$  modes, are associated to a lepton with opposite charge in order to select  $\Lambda_b^0 \rightarrow \Lambda_c^+ l^- \bar{\nu}_l$  decays. From a combined likelihood and event rate fit to the distribution of the Isgur-Wise variable  $w$ , and using the Heavy Quark Effective Theory (HQET), the slope of the  $b$ -baryon form factor is measured to be :

$$\hat{\rho}^2 = 2.03 \pm 0.46 \text{ (stat)}_{-1.00}^{+0.72} \text{ (syst)}.$$

The exclusive semileptonic branching fraction  $Br(\Lambda_b^0 \rightarrow \Lambda_c^+ l^- \bar{\nu}_l)$  can be derived from  $\hat{\rho}^2$  and is found to be  $(5.0_{-0.8}^{+1.1} \text{ (stat)}_{-1.2}^{+1.6} \text{ (syst)})\%$ . Limits on other branching fractions are also obtained.

(Phys. Lett. B585 (2004) 63-84)

J.Abdallah<sup>25</sup>, P.Abreu<sup>22</sup>, W.Adam<sup>51</sup>, P.Adzic<sup>11</sup>, T.Albrecht<sup>17</sup>, T.Alderweireld<sup>2</sup>, R.Aleman-Fernandez<sup>8</sup>, T.Allmendinger<sup>17</sup>, P.P.Allport<sup>23</sup>, U.Amaldi<sup>29</sup>, N.Amapane<sup>45</sup>, S.Amato<sup>48</sup>, E.Anashkin<sup>36</sup>, A.Andreazza<sup>28</sup>, S.Andringa<sup>22</sup>, N.Anjos<sup>22</sup>, P.Antilogus<sup>25</sup>, W-D.Apel<sup>17</sup>, Y.Arnoud<sup>14</sup>, S.Ask<sup>26</sup>, B.Asman<sup>44</sup>, J.E.Augustin<sup>25</sup>, A.Augustinus<sup>8</sup>, P.Baillon<sup>8</sup>, A.Ballestrero<sup>46</sup>, P.Bambade<sup>20</sup>, R.Barbier<sup>27</sup>, D.Bardin<sup>16</sup>, G.Barker<sup>17</sup>, A.Baroncelli<sup>39</sup>, M.Battaglia<sup>8</sup>, M.Baubillier<sup>25</sup>, K-H.Becks<sup>53</sup>, M.Begalli<sup>6</sup>, A.Behrmann<sup>53</sup>, E.Ben-Haim<sup>20</sup>, N.Benekos<sup>32</sup>, A.Benvenuti<sup>5</sup>, C.Berat<sup>14</sup>, M.Berggren<sup>25</sup>, L.Berntzon<sup>44</sup>, D.Bertrand<sup>2</sup>, M.Besancon<sup>40</sup>, N.Besson<sup>40</sup>, D.Bloch<sup>9</sup>, M.Blom<sup>31</sup>, M.Bluj<sup>52</sup>, M.Bonesini<sup>29</sup>, M.Boonekamp<sup>40</sup>, P.S.L.Booth<sup>23</sup>, G.Borisov<sup>21</sup>, O.Botner<sup>49</sup>, B.Bouquet<sup>20</sup>, T.J.V.Bowcock<sup>23</sup>, I.Boyko<sup>16</sup>, M.Bracko<sup>43</sup>, R.Brenner<sup>49</sup>, E.Brodet<sup>35</sup>, P.Bruckman<sup>18</sup>, J.M.Brunet<sup>7</sup>, L.Bugge<sup>33</sup>, P.Buschmann<sup>53</sup>, M.Calvi<sup>29</sup>, T.Camporesi<sup>8</sup>, V.Canale<sup>38</sup>, F.Carena<sup>8</sup>, N.Castro<sup>22</sup>, F.Cavallo<sup>5</sup>, M.Chapkin<sup>42</sup>, Ph.Charpentier<sup>8</sup>, P.Checchia<sup>36</sup>, R.Chierici<sup>8</sup>, P.Chliapnikov<sup>42</sup>, J.Chudoba<sup>8</sup>, S.U.Chung<sup>8</sup>, K.Cieslik<sup>18</sup>, P.Collins<sup>8</sup>, R.Contri<sup>13</sup>, G.Cosme<sup>20</sup>, F.Cossutti<sup>47</sup>, M.J.Costa<sup>50</sup>, B.Crawley<sup>1</sup>, D.Crennell<sup>37</sup>, J.Cuevas<sup>34</sup>, J.D'Hondt<sup>2</sup>, J.Dalmau<sup>44</sup>, T.da Silva<sup>48</sup>, W.Da Silva<sup>25</sup>, G.Della Ricca<sup>47</sup>, A.De Angelis<sup>47</sup>, W.De Boer<sup>17</sup>, C.De Clercq<sup>2</sup>, B.De Lotto<sup>47</sup>, N.De Maria<sup>45</sup>, A.De Min<sup>36</sup>, L.De Paula<sup>48</sup>, L.Di Ciaccio<sup>38</sup>, A.Di Simone<sup>39</sup>, K.Doroba<sup>52</sup>, J.Drees<sup>53,8</sup>, M.Dris<sup>32</sup>, G.Eigen<sup>4</sup>, T.Ekelof<sup>49</sup>, M.Ellert<sup>49</sup>, M.Elsing<sup>8</sup>, M.C.Espirito Santo<sup>22</sup>, G.Fanourakis<sup>11</sup>, D.Fassouliotis<sup>11,3</sup>, M.Feindt<sup>17</sup>, J.Fernandez<sup>41</sup>, A.Ferrer<sup>50</sup>, F.Ferro<sup>13</sup>, U.Flagmeyer<sup>53</sup>, H.Foeth<sup>8</sup>, E.Fokitis<sup>32</sup>, F.Fulda-Quenzer<sup>20</sup>, J.Fuster<sup>50</sup>, M.Gandelman<sup>48</sup>, C.Garcia<sup>50</sup>, Ph.Gavillet<sup>8</sup>, E.Gazis<sup>32</sup>, R.Gokieli<sup>8,52</sup>, B.Golob<sup>43</sup>, G.Gomez-Ceballos<sup>41</sup>, P.Goncalves<sup>22</sup>, E.Graziani<sup>39</sup>, G.Grosdidier<sup>20</sup>, K.Grzelak<sup>52</sup>, J.Guy<sup>37</sup>, C.Haag<sup>17</sup>, A.Hallgren<sup>49</sup>, K.Hamacher<sup>53</sup>, K.Hamilton<sup>35</sup>, S.Haug<sup>33</sup>, F.Hauler<sup>17</sup>, V.Hedberg<sup>26</sup>, M.Hennecke<sup>17</sup>, H.Herr<sup>8</sup>, J.Hoffman<sup>52</sup>, S-O.Holmgren<sup>44</sup>, P.J.Holt<sup>8</sup>, M.A.Houlden<sup>23</sup>, K.Hultqvist<sup>44</sup>, J.N.Jackson<sup>23</sup>, G.Jarlskog<sup>26</sup>, P.Jarry<sup>40</sup>, D.Jeans<sup>35</sup>, E.K.Johansson<sup>44</sup>, P.D.Johansson<sup>44</sup>, P.Jonsson<sup>27</sup>, C.Joram<sup>8</sup>, L.Jungermann<sup>17</sup>, F.Kapusta<sup>25</sup>, S.Katsanevas<sup>27</sup>, E.Katsoufis<sup>32</sup>, G.Kernel<sup>43</sup>, B.P.Kersevan<sup>8,43</sup>, U.Kerzel<sup>17</sup>, A.Kiiskinen<sup>15</sup>, B.T.King<sup>23</sup>, N.J.Kjaer<sup>8</sup>, P.Kluit<sup>31</sup>, P.Kokkinias<sup>11</sup>, C.Kourkoumelis<sup>3</sup>, O.Kouznetsov<sup>16</sup>, Z.Krumstein<sup>16</sup>, M.Kucharczyk<sup>18</sup>, J.Lamsa<sup>1</sup>, G.Leder<sup>51</sup>, F.Ledroit<sup>14</sup>, L.Leinonen<sup>44</sup>, R.Leitner<sup>30</sup>, J.Lemonne<sup>2</sup>, V.Lepeltier<sup>20</sup>, T.Lesiak<sup>18</sup>, W.Liebig<sup>53</sup>, D.Liko<sup>51</sup>, A.Lipniacka<sup>44</sup>, J.H.Lopes<sup>48</sup>, J.M.Lopez<sup>34</sup>, D.Loukas<sup>11</sup>, P.Lutz<sup>40</sup>, L.Lyons<sup>35</sup>, J.MacNaughton<sup>51</sup>, A.Malek<sup>53</sup>, S.Maltezos<sup>32</sup>, F.Mandl<sup>51</sup>, J.Marco<sup>41</sup>, R.Marco<sup>41</sup>, B.Marechal<sup>48</sup>, M.Margoni<sup>36</sup>, J-C.Marin<sup>8</sup>, C.Mariotti<sup>8</sup>, A.Markou<sup>11</sup>, C.Martinez-Rivero<sup>41</sup>, J.Masik<sup>12</sup>, N.Mastroiannopoulos<sup>11</sup>, F.Matorras<sup>41</sup>, C.Matteuzzi<sup>29</sup>, F.Mazzucato<sup>36</sup>, M.Mazzucato<sup>36</sup>, R.Mc Nulty<sup>23</sup>, C.Meroni<sup>28</sup>, W.T.Meyer<sup>1</sup>, A.Miagkov<sup>42</sup>, E.Migliore<sup>45</sup>, W.Mitaroff<sup>51</sup>, U.Mjoernmark<sup>26</sup>, T.Moa<sup>44</sup>, M.Moch<sup>17</sup>, K.Moenig<sup>8,10</sup>, R.Monge<sup>13</sup>, J.Montenegro<sup>31</sup>, D.Moraes<sup>48</sup>, S.Moreno<sup>22</sup>, P.Moretini<sup>13</sup>, U.Mueller<sup>53</sup>, K.Muenich<sup>53</sup>, M.Mulders<sup>31</sup>, L.Mundim<sup>6</sup>, W.Murray<sup>37</sup>, B.Muryn<sup>19</sup>, G.Myatt<sup>35</sup>, T.Myklebust<sup>33</sup>, M.Nassiakou<sup>11</sup>, F.Navarria<sup>5</sup>, K.Nawrocki<sup>52</sup>, R.Nicolaidou<sup>40</sup>, M.Nikolenko<sup>16,9</sup>, A.Oblakowska-Mucha<sup>19</sup>, V.Obratsov<sup>42</sup>, A.Olshevski<sup>16</sup>, A.Onofre<sup>22</sup>, R.Orava<sup>15</sup>, K.Osterberg<sup>15</sup>, A.Ouraou<sup>40</sup>, A.Oyanguren<sup>50</sup>, M.Paganoni<sup>29</sup>, S.Paiano<sup>5</sup>, J.P.Palacios<sup>23</sup>, H.Palka<sup>18</sup>, Th.D.Papadopoulou<sup>32</sup>, L.Pape<sup>8</sup>, C.Parkes<sup>24</sup>, F.Parodi<sup>13</sup>, U.Parzefall<sup>8</sup>, A.Passeri<sup>39</sup>, O.Passon<sup>53</sup>, L.Peralta<sup>22</sup>, V.Perepelitsa<sup>50</sup>, A.Perrotta<sup>5</sup>, A.Petrolini<sup>13</sup>, J.Piedra<sup>41</sup>, L.Pieri<sup>39</sup>, F.Pierre<sup>40</sup>, M.Pimenta<sup>22</sup>, E.Piotto<sup>8</sup>, T.Podobnik<sup>43</sup>, V.Poireau<sup>8</sup>, M.E.Pol<sup>6</sup>, G.Polok<sup>18</sup>, P.Poropat<sup>47</sup>, V.Pozdniakov<sup>16</sup>, N.Pukhaeva<sup>2,16</sup>, A.Pullia<sup>29</sup>, J.Rames<sup>12</sup>, L.Ramler<sup>17</sup>, A.Read<sup>33</sup>, P.Rebecchi<sup>8</sup>, J.Rehn<sup>17</sup>, D.Reid<sup>31</sup>, R.Reinhardt<sup>53</sup>, P.Renton<sup>35</sup>, F.Richard<sup>20</sup>, J.Ridky<sup>12</sup>, M.Rivero<sup>41</sup>, D.Rodriguez<sup>41</sup>, A.Romero<sup>45</sup>, P.Ronchese<sup>36</sup>, E.Rosenberg<sup>1</sup>, P.Roudeau<sup>20</sup>, T.Rovelli<sup>5</sup>, V.Ruhmann-Kleider<sup>40</sup>, D.Ryabtchikov<sup>42</sup>, A.Sadovsky<sup>16</sup>, L.Salmi<sup>15</sup>, J.Salt<sup>50</sup>, A.Savoy-Navarro<sup>25</sup>, U.Schwickerath<sup>8</sup>, A.Segar<sup>35</sup>, R.Sekulin<sup>37</sup>, M.Siebel<sup>53</sup>, A.Sisakian<sup>16</sup>, G.Smadja<sup>27</sup>, O.Smirnova<sup>26</sup>, A.Sokolov<sup>42</sup>, A.Sopczak<sup>21</sup>, R.Sosnowski<sup>52</sup>, T.Spaso<sup>8</sup>, M.Stanitzki<sup>17</sup>, A.Stocchi<sup>20</sup>, J.Strauss<sup>51</sup>, B.Stugu<sup>4</sup>, M.Szczekowski<sup>52</sup>, M.Szeptycka<sup>52</sup>, T.Szumlak<sup>19</sup>, T.Tabarelli<sup>29</sup>, A.C.Taffard<sup>23</sup>, F.Tegenfeldt<sup>49</sup>, J.Timmermans<sup>31</sup>, L.Tkatchev<sup>16</sup>, M.Tobin<sup>23</sup>, S.Todorovova<sup>12</sup>, B.Tome<sup>22</sup>, A.Tonazzo<sup>29</sup>, P.Tortosa<sup>50</sup>, P.Travnicek<sup>12</sup>, D.Treille<sup>8</sup>, G.Tristram<sup>7</sup>, M.Trochimczuk<sup>52</sup>, C.Troncon<sup>28</sup>, M-L.Turluer<sup>40</sup>, I.A.Tyapkin<sup>16</sup>, P.Tyapkin<sup>16</sup>, S.Tzamarias<sup>11</sup>, V.Uvarov<sup>42</sup>, G.Valenti<sup>5</sup>, P.Van Dam<sup>31</sup>, J.Van Eldik<sup>8</sup>, A.Van Lysebetten<sup>2</sup>, N.van Remortel<sup>2</sup>, I.Van Vulpen<sup>8</sup>, G.Vegni<sup>28</sup>, F.Veloso<sup>22</sup>, W.Venus<sup>37</sup>, P.Verdier<sup>27</sup>, V.Verzi<sup>38</sup>, D.Vilanova<sup>40</sup>, L.Vitale<sup>47</sup>, V.Vrba<sup>12</sup>, H.Wahlen<sup>53</sup>, A.J.Washbrook<sup>23</sup>, C.Weiser<sup>17</sup>, D.Wicke<sup>8</sup>,

J.Wickens<sup>2</sup>, G.Wilkinson<sup>35</sup>, M.Winter<sup>9</sup>, M.Witek<sup>18</sup>, O.Yushchenko<sup>42</sup>, A.Zalewska<sup>18</sup>, P.Zalewski<sup>52</sup>, D.Zavrtanik<sup>43</sup>, V.Zhuravlov<sup>16</sup>, N.I.Zimin<sup>16</sup>, A.Zintchenko<sup>16</sup>, M.Zupan<sup>11</sup>

- 
- <sup>1</sup>Department of Physics and Astronomy, Iowa State University, Ames IA 50011-3160, USA  
<sup>2</sup>Physics Department, Universiteit Antwerpen, Universiteitsplein 1, B-2610 Antwerpen, Belgium and IIHE, ULB-VUB, Pleinlaan 2, B-1050 Brussels, Belgium  
and Faculté des Sciences, Univ. de l'Etat Mons, Av. Maistriau 19, B-7000 Mons, Belgium  
<sup>3</sup>Physics Laboratory, University of Athens, Solonos Str. 104, GR-10680 Athens, Greece  
<sup>4</sup>Department of Physics, University of Bergen, Allégaten 55, NO-5007 Bergen, Norway  
<sup>5</sup>Dipartimento di Fisica, Università di Bologna and INFN, Via Irnerio 46, IT-40126 Bologna, Italy  
<sup>6</sup>Centro Brasileiro de Pesquisas Físicas, rua Xavier Sigaud 150, BR-22290 Rio de Janeiro, Brazil and Depto. de Física, Pont. Univ. Católica, C.P. 38071 BR-22453 Rio de Janeiro, Brazil  
and Inst. de Física, Univ. Estadual do Rio de Janeiro, rua São Francisco Xavier 524, Rio de Janeiro, Brazil  
<sup>7</sup>Collège de France, Lab. de Physique Corpusculaire, IN2P3-CNRS, FR-75231 Paris Cedex 05, France  
<sup>8</sup>CERN, CH-1211 Geneva 23, Switzerland  
<sup>9</sup>Institut de Recherches Subatomiques, IN2P3 - CNRS/ULP - BP20, FR-67037 Strasbourg Cedex, France  
<sup>10</sup>Now at DESY-Zeuthen, Platanenallee 6, D-15735 Zeuthen, Germany  
<sup>11</sup>Institute of Nuclear Physics, N.C.S.R. Demokritos, P.O. Box 60228, GR-15310 Athens, Greece  
<sup>12</sup>FZU, Inst. of Phys. of the C.A.S. High Energy Physics Division, Na Slovance 2, CZ-180 40, Praha 8, Czech Republic  
<sup>13</sup>Dipartimento di Fisica, Università di Genova and INFN, Via Dodecaneso 33, IT-16146 Genova, Italy  
<sup>14</sup>Institut des Sciences Nucléaires, IN2P3-CNRS, Université de Grenoble 1, FR-38026 Grenoble Cedex, France  
<sup>15</sup>Helsinki Institute of Physics, P.O. Box 64, FIN-00014 University of Helsinki, Finland  
<sup>16</sup>Joint Institute for Nuclear Research, Dubna, Head Post Office, P.O. Box 79, RU-101 000 Moscow, Russian Federation  
<sup>17</sup>Institut für Experimentelle Kernphysik, Universität Karlsruhe, Postfach 6980, DE-76128 Karlsruhe, Germany  
<sup>18</sup>Institute of Nuclear Physics, Ul. Kawioro 26a, PL-30055 Krakow, Poland  
<sup>19</sup>Faculty of Physics and Nuclear Techniques, University of Mining and Metallurgy, PL-30055 Krakow, Poland  
<sup>20</sup>Université de Paris-Sud, Lab. de l'Accélérateur Linéaire, IN2P3-CNRS, Bât. 200, FR-91405 Orsay Cedex, France  
<sup>21</sup>School of Physics and Chemistry, University of Lancaster, Lancaster LA1 4YB, UK  
<sup>22</sup>LIP, IST, FCUL - Av. Elias Garcia, 14-1<sup>o</sup>, PT-1000 Lisboa Codex, Portugal  
<sup>23</sup>Department of Physics, University of Liverpool, P.O. Box 147, Liverpool L69 3BX, UK  
<sup>24</sup>Dept. of Physics and Astronomy, Kelvin Building, University of Glasgow, Glasgow G12 8QQ  
<sup>25</sup>LPNHE, IN2P3-CNRS, Univ. Paris VI et VII, Tour 33 (RdC), 4 place Jussieu, FR-75252 Paris Cedex 05, France  
<sup>26</sup>Department of Physics, University of Lund, Sölvegatan 14, SE-223 63 Lund, Sweden  
<sup>27</sup>Université Claude Bernard de Lyon, IPNL, IN2P3-CNRS, FR-69622 Villeurbanne Cedex, France  
<sup>28</sup>Dipartimento di Fisica, Università di Milano and INFN-MILANO, Via Celoria 16, IT-20133 Milan, Italy  
<sup>29</sup>Dipartimento di Fisica, Univ. di Milano-Bicocca and INFN-MILANO, Piazza della Scienza 2, IT-20126 Milan, Italy  
<sup>30</sup>IPNP of MFF, Charles Univ., Areal MFF, V Holesovickach 2, CZ-180 00, Praha 8, Czech Republic  
<sup>31</sup>NIKHEF, Postbus 41882, NL-1009 DB Amsterdam, The Netherlands  
<sup>32</sup>National Technical University, Physics Department, Zografou Campus, GR-15773 Athens, Greece  
<sup>33</sup>Physics Department, University of Oslo, Blindern, NO-0316 Oslo, Norway  
<sup>34</sup>Dpto. Física, Univ. Oviedo, Avda. Calvo Sotelo s/n, ES-33007 Oviedo, Spain  
<sup>35</sup>Department of Physics, University of Oxford, Keble Road, Oxford OX1 3RH, UK  
<sup>36</sup>Dipartimento di Fisica, Università di Padova and INFN, Via Marzolo 8, IT-35131 Padua, Italy  
<sup>37</sup>Rutherford Appleton Laboratory, Chilton, Didcot OX11 0QX, UK  
<sup>38</sup>Dipartimento di Fisica, Università di Roma II and INFN, Tor Vergata, IT-00173 Rome, Italy  
<sup>39</sup>Dipartimento di Fisica, Università di Roma III and INFN, Via della Vasca Navale 84, IT-00146 Rome, Italy  
<sup>40</sup>DAPNIA/Service de Physique des Particules, CEA-Saclay, FR-91191 Gif-sur-Yvette Cedex, France  
<sup>41</sup>Instituto de Física de Cantabria (CSIC-UC), Avda. los Castros s/n, ES-39006 Santander, Spain  
<sup>42</sup>Inst. for High Energy Physics, Serpukov P.O. Box 35, Protvino, (Moscow Region), Russian Federation  
<sup>43</sup>J. Stefan Institute, Jamova 39, SI-1000 Ljubljana, Slovenia and Laboratory for Astroparticle Physics, Nova Gorica Polytechnic, Kostanjevska 16a, SI-5000 Nova Gorica, Slovenia, and Department of Physics, University of Ljubljana, SI-1000 Ljubljana, Slovenia  
<sup>44</sup>Fysikum, Stockholm University, Box 6730, SE-113 85 Stockholm, Sweden  
<sup>45</sup>Dipartimento di Fisica Sperimentale, Università di Torino and INFN, Via P. Giuria 1, IT-10125 Turin, Italy  
<sup>46</sup>INFN, Sezione di Torino, and Dipartimento di Fisica Teorica, Università di Torino, Via P. Giuria 1, IT-10125 Turin, Italy  
<sup>47</sup>Dipartimento di Fisica, Università di Trieste and INFN, Via A. Valerio 2, IT-34127 Trieste, Italy and Istituto di Fisica, Università di Udine, IT-33100 Udine, Italy  
<sup>48</sup>Univ. Federal do Rio de Janeiro, C.P. 68528 Cidade Univ., Ilha do Fundão BR-21945-970 Rio de Janeiro, Brazil  
<sup>49</sup>Department of Radiation Sciences, University of Uppsala, P.O. Box 535, SE-751 21 Uppsala, Sweden  
<sup>50</sup>IFIC, Valencia-CSIC, and D.F.A.M.N., U. de Valencia, Avda. Dr. Moliner 50, ES-46100 Burjassot (Valencia), Spain  
<sup>51</sup>Institut für Hochenergiephysik, Österr. Akad. d. Wissensch., Nikolsdorfergasse 18, AT-1050 Vienna, Austria  
<sup>52</sup>Inst. Nuclear Studies and University of Warsaw, Ul. Hoza 69, PL-00681 Warsaw, Poland  
<sup>53</sup>Fachbereich Physik, University of Wuppertal, Postfach 100 127, DE-42097 Wuppertal, Germany

† deceased

# 1 Introduction

The knowledge of the  $B$ -meson form factor has recently improved thanks to a wealth of new experimental results, as reported for instance in references [1–6]. Semileptonic decays of  $B$  mesons into  $D$  and  $D^*$  final states can be understood in the context of the Heavy Quark Effective Theory (HQET), where the four form factors remaining when the lepton mass is neglected can be expressed in terms of a single Isgur-Wise function  $\xi_M$ <sup>1</sup>, which will be defined in section 2.

In this paper, the semileptonic  $b$ -baryon decay  $\Lambda_b^0 \rightarrow \Lambda_c^+ l^- \bar{\nu}_l$  (with  $l^- = e^-$  or  $\mu^-$ ) is investigated<sup>2</sup>, where the  $\Lambda_c^+$  is fully reconstructed from its decay modes into  $pK^-\pi^+$ ,  $\Lambda\pi^+\pi^+\pi^-$ , and  $pK_S^0$ . The heavy quark symmetry relates form factors of the transition  $\Lambda_b^0 \rightarrow \Lambda_c^+ l^- \bar{\nu}_l$  to a new single Isgur-Wise function  $\xi_B$ , as explained in [7–9] and predicts its absolute value when the final  $\Lambda_c^+$  is at rest in the  $\Lambda_b$  frame. After a summary of the heavy quark formalism in section 2, and a description of the relevant parts of the DELPHI detector in section 3, the selection of the different  $\Lambda_c^+$ -lepton channels candidates is described in section 4. The dominant contribution to the  $\Lambda_c^+ l^- \bar{\nu}_l$  final state is expected to come from the  $\Lambda_b^0$  baryon, and the relevant contaminations from  $B$ -mesons, from other  $b$ -baryons, or from other hadronic final states with additional pions are investigated in sections 5 and 6. In section 7 a direct determination of the semileptonic branching fraction is presented, while the fit to the distribution of the Isgur-Wise variable  $w$  is described in section 8. The semileptonic branching fraction and the  $w$  distribution are then combined into a single measurement of the slope parameter  $\hat{\rho}^2$  of the  $b$ -baryon form factor, assuming the validity of HQET predictions.

## 2 The semileptonic decay form factor of $b$ -baryons

A complete description of the form factor formalism in semileptonic decays and theoretical predictions can be found in [10–12]. The form factors are functions of the four-momentum transfer  $q^2$  in the transition, with  $q^2 = (p_l + p_{\bar{\nu}_l})^2$  where  $p_l$  and  $p_{\bar{\nu}_l}$  are the charged lepton and neutrino four-momenta, respectively. Isgur and Wise introduce the dimensionless variable  $w$ , scalar product of the four-velocities of the  $\Lambda_b^0$  and  $\Lambda_c^+$ :

$$w = v_{\Lambda_b} \cdot v_{\Lambda_c} = (m_{\Lambda_b}^2 + m_{\Lambda_c}^2 - q^2)/(2m_{\Lambda_b}m_{\Lambda_c}). \quad (1)$$

The hadronic current in the weak decay of a beauty baryon ( $J^P = 1/2^+$ ) to a charmed baryon ( $J^P = 1/2^+$ ), as in the transition  $\Lambda_b^0 \rightarrow \Lambda_c^+ W^-$ , involves six form factors, three vectors  $F_i$  and three axial-vectors  $G_i$ . In the decay  $\Lambda_b^0 \rightarrow \Lambda_c^+ l^- \bar{\nu}_l$ , the variable  $w$  ranges from 1 (highest transfer, final  $\Lambda_c^+$  at rest) to a value close to 1.44 (smallest transfer,  $q^2 = m_l^2$ ). Among the six form factors which can contribute to the semileptonic decay of  $J^P = 1/2^+$  baryons, only  $F_1$  and  $G_1$  survive in the limit of infinite  $b$  and  $c$  quark masses, the HQET limit. In addition, they are equal and can be expressed in terms of a single function  $\xi_B(w)$ .

The differential decay width of the transition  $\Lambda_b^0 \rightarrow \Lambda_c^+ l^- \bar{\nu}_l$  can be obtained from [13] in the approximation where  $m_{light}/m_Q$  terms are neglected, where  $m_{light}$  is the mass of the light quark system and  $m_Q$  stands for the heavy quark:

$$\frac{d\Gamma}{dw} = G K(w) \xi_B^2(w), \quad (2)$$

<sup>1</sup>The subscript  $M$  has been added to indicate that this form factor applies to meson decay, while the subscript  $B$  will be used for baryons.

<sup>2</sup>The notations  $\Lambda_b^0$  and  $\Lambda_c^+$  will implicitly stand for both the baryon and antibaryon, with the proper inversion of the signs of the lepton and of the  $\Lambda_c^+$  decay products.

where the constant  $G$  is:

$$G = \frac{2}{3} \frac{G_F^2}{(2\pi)^3} |V_{cb}|^2 m_{\Lambda_b}^4 r^2 \quad \text{with} \quad r = m_{\Lambda_c}/m_{\Lambda_b}, \quad (3)$$

and the kinematical factor  $K(w)$  is:

$$K(w) = P [3w(1 - 2rw + r^2) + 2r(w^2 - 1)] \quad \text{with} \quad P = m_{\Lambda_c} \sqrt{w^2 - 1}. \quad (4)$$

The Isgur-Wise function  $\xi_B(w)$  will be studied in the present paper.

In  $B$ -meson decays, another function  $\xi_M(w)$  describes the semileptonic transitions  $\bar{B} \rightarrow (D, D^*)l^-\bar{\nu}_l$ , and a Taylor expansion is usually assumed for this function:

$$\xi_M(w) = \xi_M(1) [1 - \hat{\rho}_M^2(w - 1) + \mathcal{O}((w - 1)^2)], \quad (5)$$

with  $\xi_M(1) = 1$  in the HQET limit. The quadratic terms are constrained by dispersion relations [14–16]. Taking into account ( $m_{light}/m_c$ ) corrections and perturbative QCD effects [10–12], the value of  $\xi_M(1)$  is modified in the  $B$ -meson decay channel to  $\xi_M(1) = 0.91 \pm 0.04$ . Several experimental determinations of the mesonic form factor  $\xi_M(w)$  have been performed in the channel  $\bar{B}_d^0 \rightarrow D^{*+}l^-\bar{\nu}_l$ . Different fits are performed in [4] which quotes for a constrained quadratic fit:

$$\hat{\rho}_M^2 = 1.22 \pm 0.14 \text{ (stat)}. \quad (6)$$

Another recent determination is given in [5], and earlier measurements of  $\hat{\rho}_M^2$  were performed by [1–3].

Many different parametrisations have been proposed for the baryonic function  $\xi_B(w)$ , as given in references [13,17,18]. The simplest one is chosen which remains positive in the physical  $w$  range:

$$\xi_B(w) = \xi_B(1) \times \exp[-\hat{\rho}^2(w - 1)]. \quad (7)$$

The linear and quadratic coefficients in the Taylor expansion of this function  $\xi(w)$  are (within errors) in the domain allowed by the dispersion relation constraints evaluated in [14–16].

The flavour independence of QCD implies that, as in the usual isospin symmetry,  $\xi_B(1) = 1$ . It is shown in reference [13] that the corrections in  $m_{light}/m_Q$  to this result vanish at first order for baryons (as expected from the general result of [19]), and remain small at higher order, while this is not true for mesons. The relations between the six baryonic form factors and the Isgur-Wise function  $\xi$  are however slightly modified by the small  $m_{light}/m_Q$  corrections evaluated in [13]. The perturbative QCD corrections are smaller than for mesons and will be neglected, as explained in [20]. In sections 7 and 8 of this paper where the observed exclusive semileptonic branching fraction is used to infer  $\hat{\rho}^2$ , the finite mass corrections, as given by [13], are included into the relation between the Isgur-Wise function  $\xi_B(w)$  and the semileptonic width (equation 2). These corrections are evaluated with a  $b$  quark mass  $m_b = 4.844 \text{ GeV}/c^2$ , and a charmed quark mass  $m_c = 1.35 \text{ GeV}/c^2$ , the numerical values chosen in [13].

### 3 The DELPHI detector and the simulation

The DELPHI detector and its performance have been described in detail in [21,22]. In the barrel region, a set of cylindrical detectors, with the  $z$  coordinate axis oriented

along the 1.2 T magnetic field (and the beam) direction, allows the tracking of charged particles. The silicon Vertex Detector (VD), with an intrinsic resolution of  $7.6 \mu\text{m}$  in the plane transverse to the beam axis and  $10\text{-}30 \mu\text{m}$  along the  $z$  axis, consists of three layers. The innermost and outer layers were replaced by double-sided silicon microstrips for the 1994-1995 data taking period. The Inner Detector (ID) extends between radii of 12 cm and 28 cm and gives 24 spatial measurements. The Time Projection Chamber (TPC) provides up to 16 points between 30 cm and 122 cm. The Outer Detector (OD), at a radius of 197 cm to 206 cm, consists of 5 layers of drift cells. In the plane orthogonal to the beam direction, the extrapolation accuracy at the primary vertex of hadronic charged particles is found to be  $\sqrt{20^2 + 65^2/p_t^2} \mu\text{m}$  [23], where  $p_t$  (in GeV/ $c$ ) is the momentum of the particle transverse to the beam axis.

The identification of electrons relies on the electromagnetic calorimeter in the barrel region (high density projection chamber HPC), with a relative energy resolution of 6.5% for electrons at a momentum of 45 GeV/ $c$ . Within the HPC acceptance, electrons with a momentum above 3 GeV/ $c$  are identified with an efficiency of 77%. The probability that a pion be misidentified as an electron is below 1%. The muon identification relies mainly on the muon chambers. The selection criteria used in this work ensure an efficiency of identification of 77% for a misidentification probability of 0.8%.

The identification of protons and kaons relies on the DELPHI algorithms which take into account the information provided by the Ring Imaging Cherenkov (RICH), and the  $dE/dx$  in the Time Projection Chamber (TPC). The liquid and gas radiator signals of the RICH are used when they were present, mostly in the 1994 and 1995 data samples. A neural network program is used for the identification of charged particles in the 1994 data, while in the other data samples, a simple combination of the RICH and TPC measurements are considered. The proton and kaon tracks are required to be in the barrel region, with a polar angle to the  $z$  axis fulfilling  $|\cos\theta| < 0.74$ . The efficiencies associated to proton and kaon identification have been obtained from the simulation, and corrected for the small differences between the simulation and the data. A check of the efficiency estimate was performed on dedicated samples of real data, namely  $\Lambda$  (for the proton) and reconstructed  $D^{*\pm}$  in the  $K\pi\pi$  channel (for the kaon): a good agreement was found with the simulation in the whole momentum range. The overall proton identification efficiencies are  $(24 \pm 4)\%$  (1992 data),  $(21.5 \pm 4)\%$  (1993 data), when the liquid RICH was not operating, and  $(42 \pm 2)\%$  in 1994 and 1995. The fraction of pions misidentified as protons is approximately 5% above 3 GeV/ $c$  for good operating conditions of the RICH.

Special samples of events for each potential source of  $\Lambda_c^+$ -lepton final states were generated using the JETSET 7.3 Parton Shower program [24], with a  $\Lambda_b^0$  lifetime set to 1.6 ps. The generated events were followed through the detailed detector simulation DELSIM. The background events without a true  $\Lambda_c$  were selected from the general DELPHI simulated sample of  $q\bar{q}$  events at the  $Z$ . The same sample was used to estimate the fake lepton background. These events were then processed through the same analysis chain as the real data. A reweighting of the simulated events, which were generated with a constant value  $\xi_B(w) = 1$  of the form factor, allows the observed distributions to be predicted for all variables, and the slope parameter  $\hat{\rho}^2$  to be tuned in order to reproduce the data. A reweighting was also applied to match the measured  $\Lambda_b^0$  lifetime of 1.23 ps [25].

## 4 Event selection

### 4.1 The sample of hadronic events

Hadronic  $Z$  decays collected between 1992 and 1995 were used. The centre-of-mass energy was required to lie within 2 GeV of the  $Z$  mass. Charged particles were required to have a measured momentum between 0.1 GeV/ $c$  and 50 GeV/ $c$ , a relative error on momentum less than 100%, a track length larger than 30 cm, and a distance of closest approach to the interaction point smaller than 5 cm radially, and smaller than 10 cm along the beam axis. Neutral particles were required to have an energy between 1 GeV and 30 GeV, and a polar angle between 20 and 160 degrees. They were assigned a zero mass.

Hadronic events were then selected using the previous set of charged particles with a momentum above 0.4 GeV/ $c$ . Five or more charged particles were required, carrying a total energy (assuming them to be pions) of more than  $0.12\sqrt{s}$ . A total of 3.46 million events has been obtained. In the following sections, events will be selected from this sample which contain candidates for both a  $\Lambda_c$  and a lepton.

### 4.2 Lepton selection and b-tagging

The lepton candidates had to satisfy the appropriate identification criteria, and a method relying on a neural network was used for the electron identification. The charged leptons were required to have a momentum larger than 3 GeV/ $c$  and a transverse momentum  $p_t$  with respect to the  $\Lambda_c^+$  candidates (defined in sections 4.3 to 4.5 below) larger than 0.6 GeV/ $c$ . Additional criteria were then introduced to purify the  $\Lambda_b^0$  sample:

- The mass of the  $\Lambda_c^+$ -lepton system was required to be larger than 3 GeV/ $c^2$  (for electrons), or 3.2 GeV/ $c^2$  (for muons). This selection reduces the potential contributions from semileptonic  $B$ -meson decays with baryons in the final state and from the  $\Lambda_c^+ X l^- \bar{\nu}_l$  final states of  $\Lambda_b^0$  decays. The lower momentum selection for the electron preserves the efficiency, given a lower resolution in this channel.
- The probability that all tracks in the event come from the primary vertex was required to be less than 10%, as described in [22]. The events were then considered as  $b$ -flavour candidates. This choice is the result of a compromise between the signal yield and the level of combinatorial background in the  $\Lambda_c^+$  mass window; it gives a  $b$ -tagging efficiency of 80% with a purity of 54%.
- The sign of the lepton charge must be opposite to the  $\Lambda_c^+$  charge. It can be seen in Figure 1 that there is no evidence for a  $\Lambda_c^+$  signal in the wrong charge mass distribution. The upper limit measured from the data using the wrong sign lepton rate is 7% (95% C.L.) of the right sign sample. Similar limits have been obtained from a simulated sample of  $b\bar{b}$  events: a fit to the  $\Lambda_c^+$  mass distribution of  $\Lambda_c^+ l^-$  candidates, as in the actual data analysis, gave 438  $\Lambda_c^+ l^-$  combinations. A sample of  $13 \pm 5$   $\Lambda_c^+$  candidates were associated to fake leptons. Their fraction is then  $(4.3 \pm 1.5)\%$  of the signal <sup>3</sup>.

All final states studied in the following must have a track satisfying the lepton selection requirements.

<sup>3</sup>This number has been corrected for the different rate of fake leptons in the simulation and in the real data, and it has been subtracted from the amount of candidate events in the estimates of absolute rates.

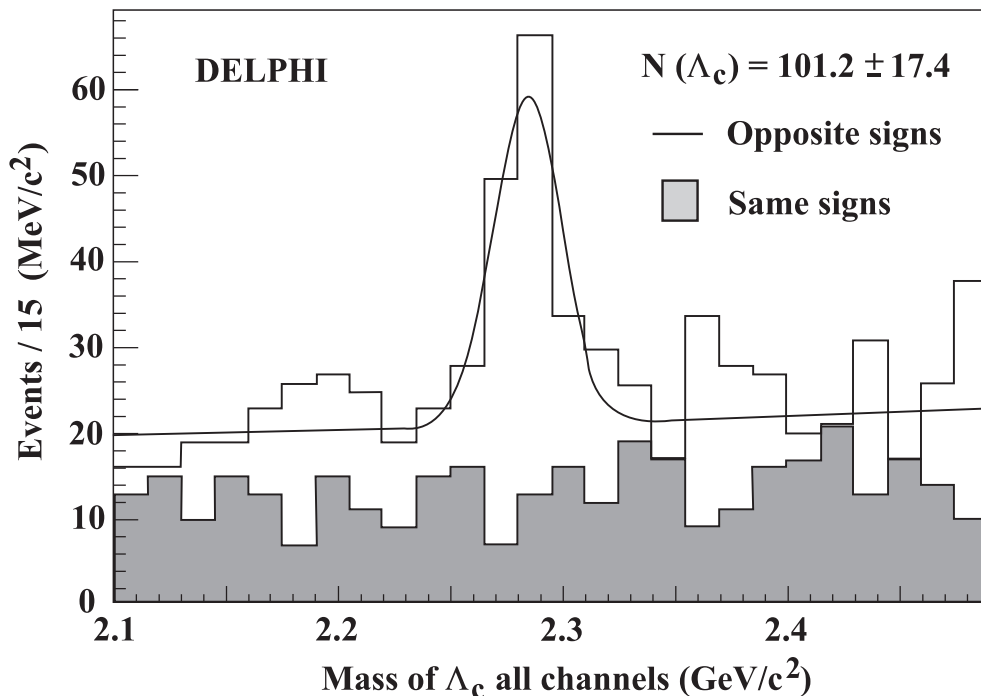


Figure 1: The  $\Lambda_c^+$  mass distribution including the decay channels  $pK^-\pi^+$ ,  $\Lambda\pi^+\pi^+\pi^-$  and  $pK_S^0$ :  $\Lambda_c^+l^-$  combinations (white histogram),  $\Lambda_c^+l^+$  combinations (hatched histogram). The curve is the sum of the fitted functions for each channel (see section 4.6).

### 4.3 $\Lambda_c^+ \rightarrow pK^-\pi^+$ selection

Triples of charged particles of total charge unity, each track with at least one hit in the microvertex detector were selected. The momenta were required to be larger than 3  $\text{GeV}/c$  (proton candidate), 2  $\text{GeV}/c$  (kaon candidate) or 1  $\text{GeV}/c$  (pion candidate), and the total momentum to be larger than 8  $\text{GeV}/c$ . The mass of the  $\Lambda_c^+$  candidate had to lie in the 2.1-2.49  $\text{GeV}/c^2$  range. A secondary vertex was fitted with these three tracks, requiring a  $\chi^2$  probability larger than 0.001. The primary vertex was found iteratively using initially all the tracks of the event and following the procedure used in [26]. The lepton track was not a priori excluded from the general vertex fit to avoid a possible bias on the lepton side. The combined  $\Lambda_b^0 - \Lambda_c^+$  flight distance was then computed as the difference between the secondary and the primary vertex. It was signed with respect to the momentum direction of the triplet, and its projection on the plane transverse to the beam axis had to be larger than +0.02 cm. The particles compatible with both  $p$  and  $K$  identifications were kept, and no identification was applied to the pion candidate. The reconstruction efficiency for this channel is 8%.

The invariant mass distribution is shown in Figure 2a. The curves in Figure 2 are obtained by fits of Gaussian distributions in the signal region, added to a linear background. The  $\Lambda_c$  mass is measured in the  $pK^-\pi^+$  channel, and fixed to the same value in the other two. The resolution  $\sigma$  of the gaussian is left free in the  $pK^-\pi^+$  channel, and found to be  $13.5 \pm 1.8 \text{ MeV}/c^2$ . The number of  $\Lambda_c^+ \rightarrow pK^-\pi^+$  events is  $80.4 \pm 15.0$ . In the other channels, discussed in the following sections, the resolution was fixed, and derived from the previous one according to the ratio of the simulated resolutions. After

reconstruction in the simulation, the gaussian resolutions are found to be 12 MeV/ $c^2$  for the  $pK^-\pi^+$  channel, 15 MeV/ $c^2$  for  $\Lambda\pi^+\pi^+\pi^-$  and 16 MeV/ $c^2$  for  $pK_S^0$ .

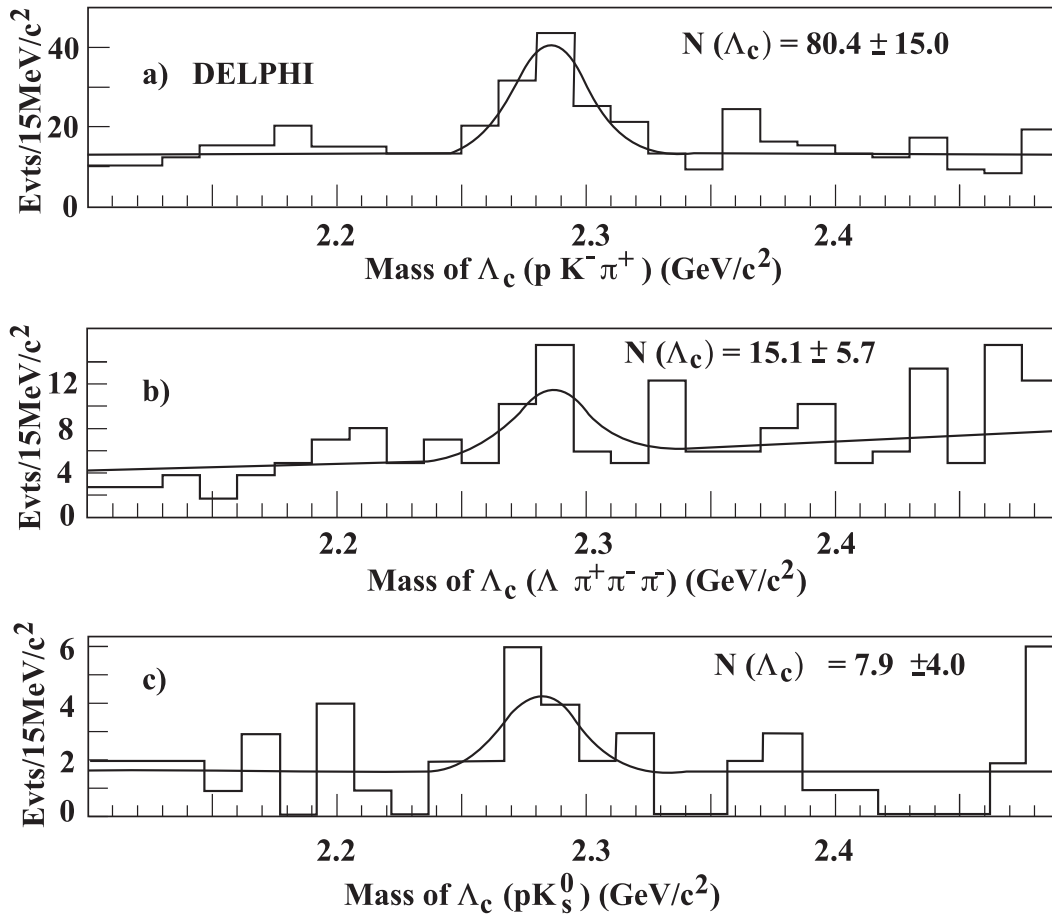


Figure 2:  $\Lambda_c^+$  mass spectrum in the a)  $pK^-\pi^+$  channel; b)  $\Lambda\pi^+\pi^+\pi^-$  channel; and c)  $pK_S^0$  channel. The fitted functions are described in section 4.3.

#### 4.4 $\Lambda_c^+ \rightarrow \Lambda\pi^+\pi^+\pi^-$ selection

The  $\Lambda$ -hyperon candidates were selected by the DELPHI algorithm which uses the presence of a remote decay vertex to tag the  $\Lambda \rightarrow p\pi^-$  candidates, as described in [22]. The hyperon and  $\Lambda_c^+$  momenta were required to be larger than 2.5 GeV/ $c$  and 10 GeV/ $c$ , respectively. All three pions were required to have a momentum larger than 0.4 GeV/ $c$ , and their tracks to have at least one associated hit in the microvertex detector. The charge of the triplet had to be +1 for  $\Lambda$  and -1 for  $\bar{\Lambda}$ , and the three pions had to form a common vertex (the  $\Lambda_c^+$  decay vertex) with a probability larger than 0.001. The projection of the flight distance of the  $\Lambda_c^+$  transverse to the beam had to be larger than +0.02 cm.

There is some evidence for a  $\Lambda_c^+$  signal in the  $\Lambda\pi^+\pi^+\pi^-$  invariant mass distribution, as shown in Figure 2b, with a fitted signal of  $15.1 \pm 5.7$   $\Lambda_c^+ \rightarrow \Lambda\pi^+\pi^+\pi^-$  candidates. All candidate combinations are shown in this figure. Some events contain more than one accepted combination, and for two events, both of them are in the  $\Lambda_c^+$  mass range  $2.260 < M(\Lambda_c^+) < 2.310$  GeV/ $c^2$ .

## 4.5 $\Lambda_c^+ \rightarrow pK_S^0$ selection

Once a  $K_S^0$  candidate had been found [22], an identified proton was searched for, such that the  $\Lambda_c$  candidate would belong to the hemisphere defined by the lepton track. The momenta of the  $K_S^0$  and proton had to be larger than 3 GeV/c. The  $(pK_S^0)$  mass distribution is shown in Figure 2c, with a fitted signal of  $7.9 \pm 4.0$  candidates.

## 4.6 The full $\Lambda_c^+ l^-$ sample

The ratios of the number of events obtained in the three channels are compatible with the known  $\Lambda_c^+$  branching fractions [25]. The curve in Figure 1, which shows the full  $\Lambda_c^+ l^-$  sample, is obtained from the sum of the three Gaussian functions, with their widths as indicated in section 4.3, and a unique central value. The Gaussian functions are weighted by the number of observed events in each channel, and with a free overall normalisation. The number of  $\Lambda_c^+ l^-$  candidates is found to be  $101.2 \pm 17.4$ .

## 5 Other sources of $\Lambda_c^+ l^-$ final states

There are several physical processes which lead to the  $\Lambda_c^+$ -lepton final states, in addition to the signal from  $\Lambda_b^0 \rightarrow \Lambda_c^+ l^- \bar{\nu}_l$ , named elastic channel in the following. They arise from instrumental or physical backgrounds:

- a) the semileptonic decay  $\Lambda_b^0 \rightarrow \Lambda_c^+ \tau^- \bar{\nu}_\tau$  with the subsequent decay  $\tau^- \rightarrow l^- \bar{\nu}_l \nu_\tau$ ;
- b) fake leptons: the fraction of fake leptons, estimated to be  $(4.3 \pm 1.5)\%$  in section 4.2 will be subtracted from the sample of  $\Lambda_c^+ l^-$  candidates in sections 7 and 8;
- c) decays of  $\bar{B}$  mesons:  $\bar{B} \rightarrow \Lambda_c^+ \bar{N} l^- \bar{\nu}_l (X)$ , where  $\bar{N}$  is an antibaryon and  $X$  stands for any number of  $\pi^0$  or  $(\pi^+ \pi^-)$  pair;
- d) decays into other charmed baryons  $\Lambda_b^0 \rightarrow \Lambda_c^{*+} l^- \bar{\nu}_l$ , or  $\Lambda_b^0 \rightarrow (\Sigma_c \pi)^+ l^- \bar{\nu}_l$ ;
- e) non-resonant  $\Lambda_c^+ l^- \bar{\nu}_l X$  final states. The multiplicity  $N_c$  of charged particle tracks compatible with the  $\Lambda_b^0$  vertex, defined as the combined  $(\Lambda_c l)$  vertex (ignoring the  $\Lambda_c$  lifetime), the missing mass in the  $\Lambda_b^0$  decay, and the  $\Lambda_c^+ l^-$  mass will be used to investigate this component, including as well the decays from d). The sum of d) and e) final states is named inelastic channels in the following;
- f) other weakly decaying  $b$ -baryons, such as  $\Xi_b$ . The production rate of  $\Xi_b$  from  $b$  quarks is however 10 times lower than the  $\Lambda_b$  production (as discussed in section 7), and the fraction of  $\Lambda_c$  final states from  $\Xi_b$ , if assumed to be similar to that of  $\Xi_c$  decays into  $\Lambda$  baryons, is also less than 10%. This background has thus been neglected.

The final states b) to f) are background processes, while the  $\tau$  lepton final state a), belongs to the signal. Its contribution was estimated with the full simulation of the decay  $\Lambda_b^0 \rightarrow \Lambda_c^+ \tau^- \bar{\nu}_\tau$ , assuming the same couplings as for the other leptons. The branching fraction is found to be six times smaller than for  $\Lambda_c^+ l^- \bar{\nu}_l$  with light leptons. The observed  $\tau$  contribution is further suppressed by the lepton momentum selections. The estimated yield amounts to 2 events in the full  $\Lambda_c^+$  sample of 101 events and can be neglected.

The number of events from the decay of  $\bar{B}$  mesons in the  $\Lambda_c^+$  sample was computed with the full simulation, using the value quoted in [25]:  $Br(\bar{B} \rightarrow \Lambda_c^+ \bar{N} l^- \bar{\nu}_l) < 0.0032$  at the 90% C.L., which relies on the data from [27]. The contamination of such decays into the sample of  $\Lambda_c^+ l^- \bar{\nu}_l$  events is found to be less than 1.5 events (90% C.L.). The inclusive final states with an additional charged or neutral pion have a branching fraction smaller than 0.0064 [25], and their acceptance is found from the simulation to be smaller by a

factor 0.62, so that they can contribute up to 1.9 events. The total contamination of  $\Lambda_c^+ \bar{N} X l^- \bar{\nu}_l$  events from  $\bar{B}$  mesons into the  $\Lambda_c^+ l^-$  sample is thus estimated to be less than 3.4 events (90% C.L.).

## 6 Charmed baryon contributions to b-baryon decays

To extract the form factor corresponding to the  $\Lambda_b^0 \rightarrow \Lambda_c^+ l^- \bar{\nu}_l$  decays from the  $\Lambda_c^+ l^-$  sample, the contributions arising from the elastic and inelastic channels must be evaluated. Whether resonant charmed hadrons are present in the corresponding mass spectra is investigated first: if there is a large and dominant resonant contribution, its production should be described by the appropriate form factors. As shown in the following, no signal is observed and the corresponding upper limits will be given. Other experimental distributions which are sensitive to the fraction of inelastic channels in the sample are also considered. As it will be shown, they can only be understood under the assumption of a substantial contribution from inelastic  $\Lambda_c^+ \pi \pi$  final states.

### 6.1 The resonant states

In addition to the elastic  $\Lambda_c^+ l^- \bar{\nu}_l$  channel, several charmed baryon final states can contribute to the  $\Lambda_c^+ l^-$  sample, such as  $(\Sigma_c \pi)^+ X l^- \bar{\nu}_l$ , and  $\Lambda_c^{*+} X l^- \bar{\nu}_l$ , in which the  $\Sigma_c$  and  $\Lambda_c^{*+}$  decay into a  $\Lambda_c^+$ .

The isospin of the hadronic final state should be  $I = 0$  within HQET. In this section, the presence of the HQET-allowed hadronic final states which correspond to the following decay channels, all with a  $\Lambda_c^+ \pi \pi$  final state, are investigated:

- $\Lambda_b^0 \rightarrow \Sigma_c^{++} \pi^- l^- \bar{\nu}_l$ , with  $\Sigma_c^{++} \rightarrow \Lambda_c^+ \pi^+$ ;
- $\Lambda_b^0 \rightarrow \Sigma_c^0 \pi^+ l^- \bar{\nu}_l$ , with  $\Sigma_c^0 \rightarrow \Lambda_c^+ \pi^-$ ;
- $\Lambda_b^0 \rightarrow \Sigma_c^+ \pi^0 l^- \bar{\nu}_l$ , with  $\Sigma_c^+ \rightarrow \Lambda_c^+ \pi^0$ ;
- $\Lambda_b^0 \rightarrow \Lambda_c^{*+} l^- \bar{\nu}_l$ , with  $\Lambda_c^{*+} \rightarrow \Lambda_c^+ \pi^+ \pi^-$ , or  $\Lambda_c^+ \pi^0 \pi^0$ .

The search for resonant states described in this section is not sensitive to channels with  $\pi^0$ 's. The first three decay modes are expected to have the same branching fractions. The  $\Sigma_c(2455)$  and  $\Sigma_c(2520)$  resonances would show up as peaks in the distribution of the variable  $Q_\Sigma$ , defined as:

$$Q_\Sigma = M(\Lambda_c^+ \pi) - M(\Lambda_c^+) - m_\pi. \quad (8)$$

As the relative sign between the  $\Lambda_c^+$  and the charged pion has not been distinguished, the  $Q_\Sigma$  distribution should contain the same number of events from  $\Lambda_b^0 \rightarrow \Sigma_c^{++} \pi^- l^- \bar{\nu}_l$ , and  $\Lambda_b^0 \rightarrow \Sigma_c^0 \pi^+ l^- \bar{\nu}_l$ , and the same combinatorial background. For display purposes, the expected spectrum for the decay  $\Lambda_b^0 \rightarrow (\Sigma_c(2455)\pi) l^- \bar{\nu}_l$  is shown as a dashed line in Figure 3, under the assumption that the observed number of events satisfies:

$$\frac{N_{obs}(\Lambda_b^0 \rightarrow \Sigma_c^{++} \pi^- l^- \bar{\nu}_l) + N_{obs}(\Lambda_b^0 \rightarrow \Sigma_c^0 \pi^+ l^- \bar{\nu}_l)}{N_{obs}(\Lambda_b^0 \rightarrow \Lambda_c^+(X) l^- \bar{\nu}_l)} = 0.1 \quad (9)$$

where the denominator is the total number of events in the  $\Lambda_c^+ l^-$  sample. The  $\Sigma_c(2520)$  signal, indicated as a dotted line histogram, is broadened due to its natural width of 20 MeV/ $c^2$ .

From the number  $N_{obs}$  of events found in the signal region  $Q_\Sigma$  (column 3 of Table 1), upper limits have been derived on the number of observable decays from the  $\Lambda_b^0 \rightarrow$

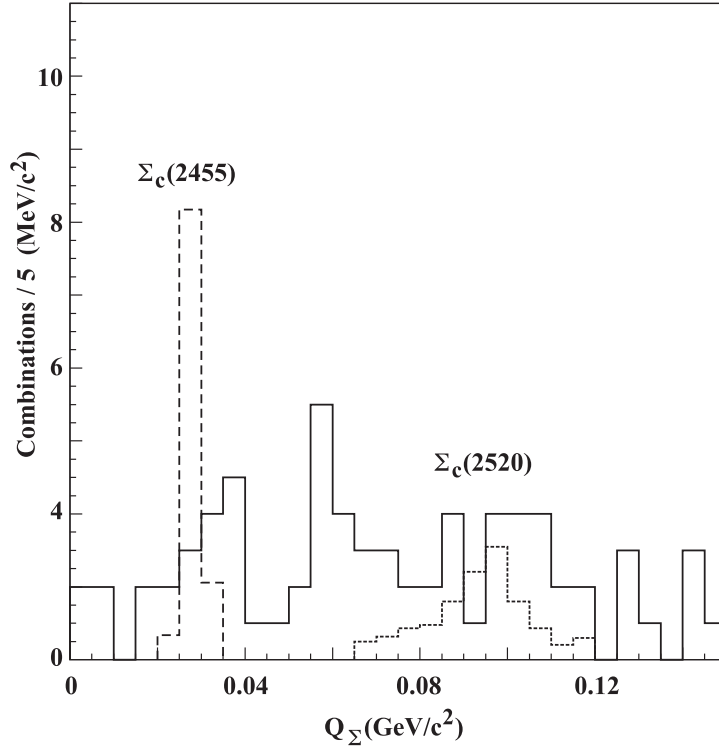


Figure 3: *Distribution of  $Q_\Sigma = M(\Lambda_c^+ \pi) - M(\Lambda_c^+) - m_\pi$  in data (solid line histogram). The simulated  $\Sigma_c(2455)$  (dashed line histogram) and  $\Sigma_c(2520)$  (dotted line histogram) signals each assume  $N_{obs}(\Lambda_b^0 \rightarrow \Sigma_c^{++} \pi^- l^- \bar{\nu}_l) + N_{obs}(\Lambda_b^0 \rightarrow \Sigma_c^0 \pi^+ l^- \bar{\nu}_l) = 0.1 N_{obs}(\Lambda_c^+(X) l^- \bar{\nu}_l)$ .*

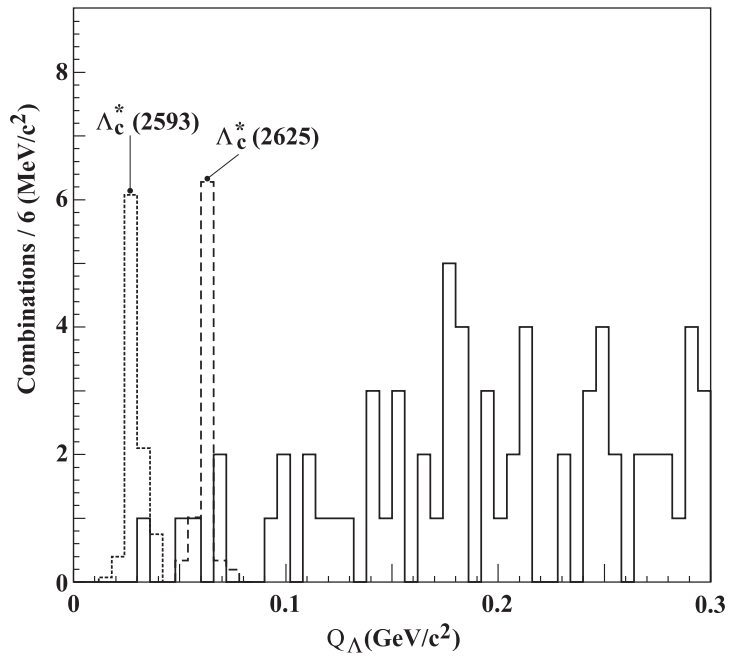


Figure 4: *Distribution of  $Q_\Lambda = M(\Lambda_c^+ \pi \pi) - M(\Lambda_c^+) - 2m_\pi$  in data (solid line histogram). The simulated  $\Lambda_c^*$  signals (dotted and dashed line histograms) assume  $N_{obs}(\Lambda_b^0 \rightarrow \Lambda_c^{*+} l^- \bar{\nu}_l) = 0.1 N_{obs}(\Lambda_c^+(X) l^- \bar{\nu}_l)$ .*

Decay channel	$Q_B$ window (GeV/c <sup>2</sup> )	$N_{obs}$ observed	$N_{bkg}$ estimated	$N_{limit}$ upper	limit on $R_{channel}$
$\Lambda_b^0 \rightarrow \Sigma_c(2455)^{++}\pi^-l^-\bar{\nu}_l +$ $\Lambda_b^0 \rightarrow \Sigma_c(2455)^0\pi^+l^-\bar{\nu}_l$	0.025-0.030	3	2.5	5.30	0.078
$\Lambda_b^0 \rightarrow \Sigma_c(2520)^{++}\pi^-l^-\bar{\nu}_l +$ $\Lambda_b^0 \rightarrow \Sigma_c(2520)^0\pi^+l^-\bar{\nu}_l$	0.080-0.105	15	10.5	12.5	0.190
$\Lambda_b^0 \rightarrow \Lambda_c(2593)^{*+}l^-\bar{\nu}_l$	0.024-0.036	1	0.5	4.30	0.064
$\Lambda_b^0 \rightarrow \Lambda_c(2625)^{*+}l^-\bar{\nu}_l$	0.054-0.066	1	1.5	3.20	0.048

Table 1:  $Q_B$  window ( $B = \Sigma, \Lambda$ ), number of observed events  $N_{obs}$ , estimated number of background events  $N_{bkg}$ , 95% C.L. upper limit on the observable number of signal events  $N_{limit}$ , and the upper limit on the channel contribution to the observed sample  $R_{channel}$ .

( $\Sigma_c\pi$ )<sup>+</sup> $l^-\bar{\nu}_l$  channels (Table 1). These limits are obtained from the highest expected yield of signal events,  $\bar{N}_\Sigma$ , such that the probability:

$$Prob(N_\Sigma + N_{bkg} \leq N_{obs}) > 5\%. \quad (10)$$

The probability law for the number of events is assumed to be a Poisson law, with the mean given by the sum of the background contribution  $\bar{N}_{bkg}$ , interpolated from the adjacent bins of the  $Q_\Sigma$  spectrum, and  $\bar{N}_\Sigma$ , the expected yield. The uncertainty on the estimated mean background level has not been included.

To search for the  $\Lambda_c^{*+}$  states, the distribution of the variable

$$Q_\Lambda = M(\Lambda_c^+\pi^+\pi^-) - M(\Lambda_c^+) - 2m_\pi \quad (11)$$

is considered (see Figure 4), and 95% C.L. upper limits have been obtained using the same procedure as in the ( $\Sigma\pi$ ) final states. The kinematical window for  $Q_\Lambda$  is given by the column 2 of Table 1.

The upper limits in column 5 of Table 1 refer to the observable final states. The contributing fraction  $R_{channel}$  in column 6 is:

$$R_{channel} = \frac{N_{channel}}{N_{obs}(\Lambda_c^+(X)l^-\bar{\nu}_l)} \quad (12)$$

where  $N_{channel}$  is the (maximal) number of events from this channel contributing to the  $\Lambda_c^+l^-$  sample: a correction factor of 3/2 has been applied to the upper limits for the  $\Lambda_c^{*+}$  final states, as the pion pair is assumed to have  $I = 0$ . The same factor 3/2 has been applied to the observed  $\Sigma_c^+$  contribution in order to include the  $\Lambda_c^+\pi^0$  final state.

## 6.2 The $\Lambda_c^+\pi\pi$ contribution

No evidence for the production of excited charmed states in  $\Lambda_b^0$  semileptonic decay has been found, but the limits obtained still allow for a substantial contribution from these final states. As, in addition, non-resonant charmed channels might be present, an inclusive approach will be adopted to evaluate the combined contribution of the resonant and non-resonant final states. This inelastic contribution is investigated by studying three distributions:

- the multiplicity  $N_c$  of charged particle tracks associated to the secondary vertex (Figure 5a);
- the missing mass squared  $M_{miss}^2 = (p_{\Lambda_b} - p_{\Lambda_c^+} - p_l)^2$  (Figure 5b);
- the  $\Lambda_c^+$ -lepton mass, which is expected to be smaller for  $\Lambda_c^+(\pi\pi)l^-\bar{\nu}_l$  final states (Figure 5c).

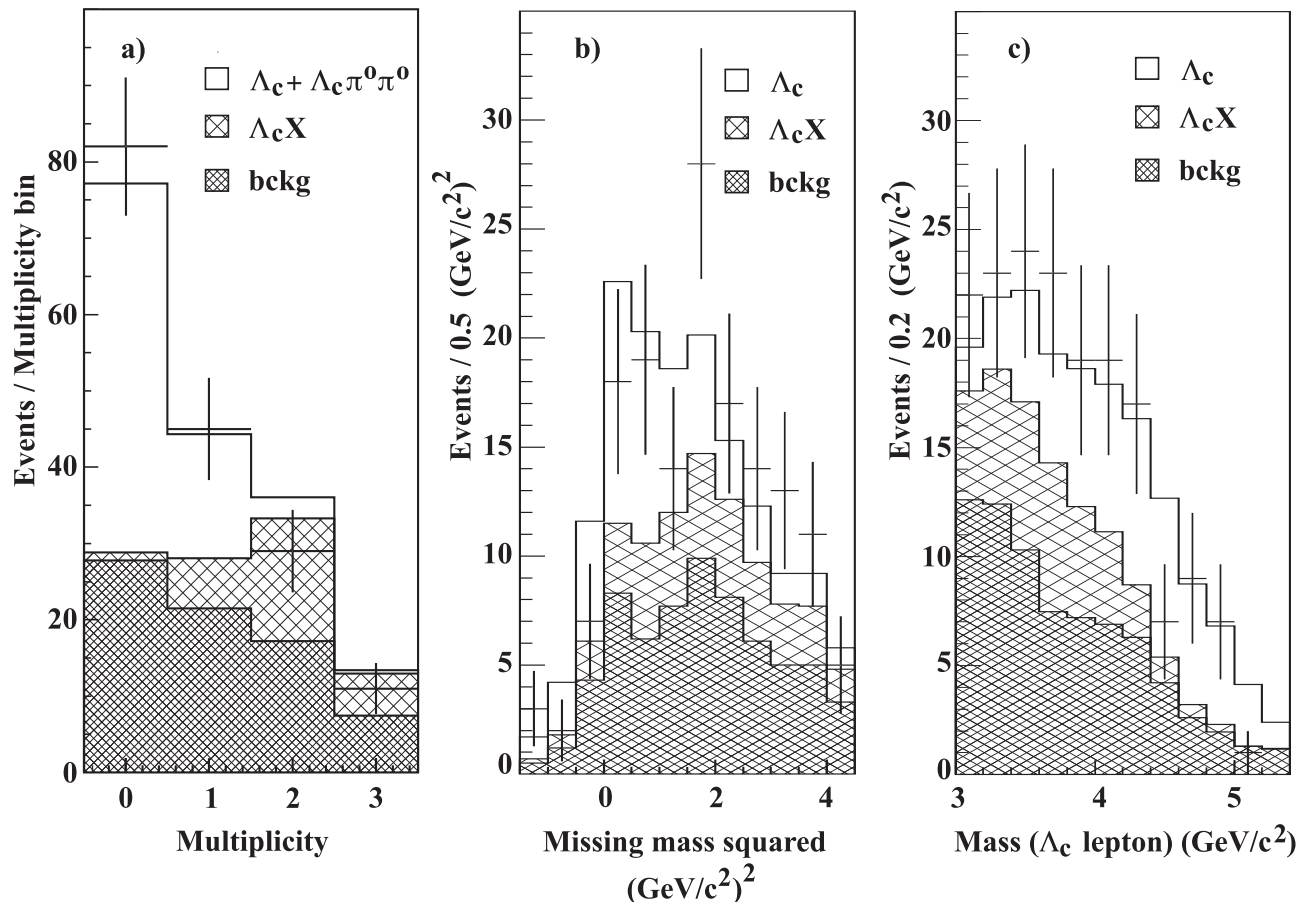


Figure 5: a) The charged multiplicity; b) the missing mass squared and c) the  $(\Lambda_c l)$  mass distributions in the  $\Lambda_c^+$  mass window. The hatched areas show the  $\Lambda_c^+ \pi^+ \pi^-$  contributions (including  $\pi^0 \pi^0$ ). The cross hatched histogram is the combinatorial background.

### 6.2.1 The multiplicity

The multiplicity of charged particles other than the  $\Lambda_c^+$  decay products and the lepton, compatible with the  $\Lambda_b^0$  vertex was evaluated by a neural network algorithm which separates tracks compatible with the primary or the secondary vertex. The probability of the vertex assignment was required to be larger than 0.5. The  $b$  and  $c$  vertices were not separated in this treatment. The result for the events situated in the  $\Lambda_c^+$  mass window  $2.260 \text{ GeV}/c^2 < M_{\Lambda_c} < 2.310 \text{ GeV}/c^2$  is shown in Figure 5a. The contribution of the  $\Lambda_c^+ \pi^0 \pi^0 l^-\bar{\nu}_l$  channel is assumed to be 1/2 of the charged pion mode  $\Lambda_c^+ \pi^+ \pi^- l^-\bar{\nu}_l$ , as the hadronic state is assumed to have  $I = 0$ .

### 6.2.2 The missing mass in $\Lambda_b^0 \rightarrow \Lambda_c^+ l^- \bar{\nu}_l$

To reconstruct the missing mass squared  $M_{miss}^2$ , with  $M_{miss}^2 = (p_{\Lambda_b} - p_{\Lambda_c} - p_l)^2$ , the four-momentum of the  $\Lambda_b^0$  was evaluated assuming the decay channel  $\Lambda_b^0 \rightarrow \Lambda_c^+ l^- \bar{\nu}_l$ . The energy is  $E_{\Lambda_b} = E_{\Lambda_c} + E_l + E_{\nu}$ , and the  $\Lambda_b^0$  momentum has been computed as  $\sqrt{E_{\Lambda_b}^2 - m_{\Lambda_b}^2}$  with  $m_{\Lambda_b} = 5.624 \text{ GeV}/c^2$ . The neutrino energy and the direction of the  $\Lambda_b^0$  have to be determined. The energy of the undetected neutrino in the exclusive  $\Lambda_b^0 \rightarrow \Lambda_c^+ l^- \bar{\nu}_l$  channel was estimated as in previous studies of semileptonic decay of  $B$  mesons [1]. The total energy in the  $\Lambda_c^+ l^-$  hemisphere, which is the sum of the visible energy ( $E_{same}$ ) in the same hemisphere, and of the neutrino energy ( $E_{miss}$ ), was computed using the observed total masses of the  $\Lambda_c^+$  hemisphere ( $M_{same}$ ) and of the opposite hemisphere ( $M_{oppo}$ ), together with four-momentum conservation:

$$E_{miss} + E_{same} = \frac{\sqrt{s}}{2} + \frac{M_{same}^2 - M_{oppo}^2}{2\sqrt{s}}. \quad (13)$$

As  $E_{same}$ ,  $M_{same}$ , and  $M_{oppo}$ , are approximately known due to the detector inefficiencies, an empirical correction  $f_{sim}(E_{same})$  (as in [1]) has been estimated from a simulation of the exclusive semileptonic channel, to improve the accuracy on the neutrino energy reconstruction:

$$E_{\bar{\nu}_l} = E_{miss} + f_{sim}(E_{same}). \quad (14)$$

Whenever this procedure leads to a negative energy, the value  $E_{\bar{\nu}_l} = 0$  is used. The final resolution on the neutrino energy is around 33%. Adding this energy to the energy of the  $\Lambda_c^+$  and of the lepton gives the energy of the  $\Lambda_b^0$  with a resolution of 8% (Gaussian fit). The direction of the  $\Lambda_b^0$  can be estimated by two different methods: the momentum of the  $\Lambda_c^+ l^-$  system gives the best accuracy when the line of flight is short, while the positions of the primary and secondary vertices, work best at large separations. In the data from 1992 and 1993, where the microvertex detector did not provide any  $z$  information, the  $\Lambda_c^+ l^-$  momentum was always used to measure the polar angle  $\theta$ . The weighted combination of the two which gave the best resolution on the Isgur-Wise variable  $w$  was chosen.

It is seen in Figure 5b that the reconstructed missing mass squared  $M_{miss}^2$  is sensitive to the presence of the inelastic channel.

### 6.2.3 The $\Lambda_c^+ l^-$ mass

The  $\Lambda_c^+ l^-$  mass distribution is expected to be shifted to lower values in the inelastic  $\Lambda_c^+ \pi \pi l^- \bar{\nu}_l$  final states. This effect is apparent in Figure 5c and it constrains the proportion of inelastic events

### 6.2.4 Fit of the elastic fraction $f_{\Lambda_c}$

To measure the fraction  $f_{\Lambda_c}$  of elastic  $\Lambda_c^+ l^- \bar{\nu}_l$  decays, the three previous distributions are considered to be the sum of three components:

- the  $\Lambda_b^0 \rightarrow \Lambda_c^+ l^- \bar{\nu}_l$  decays;
- the  $\Lambda_b^0 \rightarrow \Lambda_c^+ \pi \pi l^- \bar{\nu}_l$  decays. As this channel is a sum of many states, it is simulated without a form factor, using the quark matrix elements for weak decays in PYTHIA [28];
- events from the combinatorial background present under the  $\Lambda_c^+$  signal. The shape of this component is evaluated using events situated in the side bands of the  $\Lambda_c$  mass peak. Its normalisation is fixed according to the fit of Figure 1.

The overall normalisation is fixed to the total number of observed events. The elastic fraction  $f_{\Lambda_c}$  in the final state is obtained from three fits to the three distributions in Figures 5. Each of them is first adjusted independently. The statistical correlations of the three results are obtained from the simulated two dimensional distributions of the three pairs of variables. They are respectively: 0.25 for (multiplicity,  $\Lambda_c^+ l^-$  mass), 0.35 for (multiplicity, missing mass), and 0.65 for (missing mass,  $\Lambda_c^+ l^-$  mass). The combined fit to the three values gives:

$$f_{\Lambda_c} = \frac{N(\Lambda_c^+ l^- \bar{\nu}_l)}{N(\Lambda_c^+ l^- \bar{\nu}_l) + N(\Lambda_c^+ \pi \pi l^- \bar{\nu}_l)} = 0.60 \pm 0.08 \text{ (stat)} \pm 0.06 \text{ (syst)}. \quad (15)$$

The ratio  $f_{\Lambda_c}$  is *not* a branching fraction, but the ratio of the observed contributions in the data sample. The systematic uncertainties arising from the identification efficiency, the time of flight and the modelling of the  $b$ -quark fragmentation are negligible. The uncertainty on  $\hat{\rho}^2$ , as measured in this paper, changes  $f_{\Lambda_c}$  by  $\pm 0.02$ , and the uncertainty from the simulation of the inelastic channels is estimated to be  $\pm 0.03$  by substituting a  $\Sigma_c \pi$  decay for the  $\Lambda_c^+ \pi \pi$  non-resonant prediction. The systematic uncertainty from the combinatorial background is estimated by comparing side bands of different sizes and contributes  $\pm 0.05$ . The limits on the observed resonance contributions given in section 6.1 can be turned into limits on branching fractions. The fraction of observable decays can be derived from the assumption of an  $I = 0$  final state and is found, as already mentioned, to be  $2/3$ . The kinematical acceptances for  $(\Sigma_c \pi, \Lambda_c^*) l^- \bar{\nu}_l$  and  $\Lambda_c^+ l^- \bar{\nu}_l$  in the charged decay channels differ, with  $\epsilon(\Lambda_c^+(\pi^+ \pi^-) l^- \bar{\nu}_l) / \epsilon(\Lambda_c^+ l^- \bar{\nu}_l) = 0.57$ , according to the simulation. The branching fraction to the exclusive  $\Lambda_c^+ l^- \bar{\nu}_l$  final state can then be estimated to be:

$$\frac{\Gamma(\Lambda_b^0 \rightarrow \Lambda_c^+ l^- \bar{\nu}_l)}{\Gamma(\Lambda_b^0 \rightarrow \Lambda_c^+ l^- \bar{\nu}_l) + \Gamma(\Lambda_b^0 \rightarrow \Lambda_c^+ \pi \pi l^- \bar{\nu}_l)} = 0.47_{-0.08}^{+0.10} \text{ (stat)}_{-0.06}^{+0.07} \text{ (syst)}. \quad (16)$$

Although half of the  $\Lambda_c^+ l^-$  events in the  $\Lambda_b^0$  decay arise from a  $\Lambda_c^+ \pi \pi l^- \bar{\nu}_l$  final state, no signal from resonant production of  $\Sigma_c$  or  $\Lambda_c^*$  has been observed in the present sample.

## 7 Leptonic branching fraction from the event rate

The previous determination of the fraction of elastic semileptonic decays of  $\Lambda_b^0 \rightarrow \Lambda_c^+ l^- \bar{\nu}_l$  in the  $\Lambda_c^+ l^-$  sample allows a measurement of the semileptonic branching fraction,  $B_{\Lambda_c}$ , in this transition. As the total width of the  $\Lambda_b^0$  is given by its lifetime, this branching fraction can then provide a direct measurement of the slope parameter  $\hat{\rho}^2$  of the form factor. The branching fraction  $B_{\Lambda_c}$  has been measured from the number of  $\Lambda_b^0 \rightarrow \Lambda_c^+ l^- \bar{\nu}_l$  candidates using only the decay channel  $\Lambda_c^+ \rightarrow p K^- \pi^+$ , which has less background:

$$N(\Lambda_c^+ l^- \bar{\nu}_l) = N_Z^h 2 R_b f(b \rightarrow \Lambda_b^0) B_{\Lambda_c} Br(\Lambda_c^+ \rightarrow p K^- \pi^+) \epsilon(p K \pi l) N_l. \quad (17)$$

As the event rate is much more sensitive than the  $w$  shape to the knowledge of the identification efficiencies, this analysis has been restricted to the periods of data taking where both gas and liquid RICH were present. The number of hadronic  $Z$  decays is  $N_Z^h = 1.52 \times 10^6$ , and the fraction of  $b$ -flavoured final states is  $R_b = 0.217$  [25]. Detailed comparisons have shown that the identification efficiencies in data and simulation are then in excellent agreement. The simulated reconstruction and identification efficiency is found to be, including the lepton,  $\epsilon(p K \pi l) = (8.0 \pm 0.8)\%$ . The branching fraction  $Br(\Lambda_c^+ \rightarrow p K^- \pi^+) = (5.0 \pm 1.3)\%$ , and  $f(b \rightarrow \Lambda_b^0) = 0.108 \pm 0.020$  (subtracting 1% for  $\Xi_b$  from the quoted value in [25]) are used. The number of lepton families is  $N_l = 2$ , as the

reference value	$\pm$ uncertainty range	$\delta B_{\Lambda_c}/B_{\Lambda_c}$
$Br(\Lambda_c^+ \rightarrow pK^- \pi^+) = 0.050$	0.013	0.26
$f(b \rightarrow \Lambda_b^0) = 0.108$	0.020	0.18
$f_{\Lambda_c} = 0.60$	0.10	0.16
$\epsilon(pK\pi l) = 0.080$	0.008	0.11
$\tau_{\Lambda_b} = 1.23$ ps	0.08 ps	0.065
$B$ meson decays < 3.4%	0.034	0.034
fake leptons = 4.3%	1.5%	0.016
<b>Total</b> ( $\delta B_{\Lambda_c}/B_{\Lambda_c}$ )		0.37

Table 2: *Main sources of systematic uncertainties on the expected rate.*

$\tau$  contribution is negligible. The total number of observed  $\Lambda_c^+ l^- \bar{\nu}_l$  and  $\Lambda_c^+ X l^- \bar{\nu}_l$  events (without the enrichment selections for the elastic channel of section 8) is  $47 \pm 10$ . The fake lepton contamination, as determined in section 4.2 amounts to  $2.0 \pm 0.7$  events and should be subtracted. The “observed” number  $N(\Lambda_c^+ l^- \bar{\nu}_l)$  of exclusive  $\Lambda_c^+ l^- \bar{\nu}_l$  decays can be estimated from the latter fraction to be  $N_{obs} = f_{\Lambda_c} \cdot (47 - 2.0) = 27 \pm 6$ . This implies  $B_{\Lambda_c} = (4.7 \pm 1.1$  (stat))%. The main sources of systematic errors on  $B_{\Lambda_c}$  are given in Table 2 and sum to a relative error of 37%, so that:

$$B_{\Lambda_c} = (4.7 \pm 1.1$$
 (stat)  $\pm 1.7$  (syst))%. (18)

Most of the systematic error arises from the uncertainty on  $Br(\Lambda_c^+ \rightarrow pK^- \pi^+)$ . The other systematic errors include the uncertainty on the reconstruction efficiency  $\epsilon$ , including identification, the contribution of the  $B$ -meson decays which was varied up to the maximal value of 3.4% found in section 5. The impact of the lifetime uncertainty on the acceptance is negligible, but its effect on the parameter  $\hat{\rho}^2$  via the normalisation of the branching fraction is large and it is included here to simplify the presentation. The contribution of the  $pK^- \pi^+$  branching ratio can be explicitly extracted:

$$B_{\Lambda_c} = (4.7 \pm 1.1$$
 (stat)  $\pm 1.3$  ( $Br(\Lambda_c \rightarrow pK^- \pi^+)$ )  $\pm 1.3$  (other syst))%. (19)

The semileptonic decay width can be computed from  $\hat{\rho}^2$ , using equation (2), under the assumption that  $\xi_B(1) = 1$ . The total width is given by the  $\Lambda_b^0$  lifetime  $\tau_{\Lambda_b} = 1.23 \pm 0.08$  ps [25], and the semileptonic branching fraction  $B_{\Lambda_c}$  provides (within HQET) an estimate of the slope  $\hat{\rho}^2$ :

$$\hat{\rho}_{rate}^2 = 2.05_{-0.50}^{+0.70}$$
 (stat error only). (20)

This measurement of  $\hat{\rho}^2$  will be combined in the next section with a fit to the distribution of the Isgur-Wise variable  $w$  to obtain an improved determination of the slope parameter and of the branching fraction. The impact of systematic errors will be evaluated for this combined fit.

## 8 Combined fit to the $w$ shape and the event rate

### 8.1 The enriched $\Lambda_c^+$ -lepton sample

As has been shown in Figure 1, the number of  $\Lambda_c^+$ -lepton pairs is  $101 \pm 17$ , and this sample contains the elastic  $\Lambda_c^+ l^- \bar{\nu}_l$  and inelastic  $\Lambda_c^+ (\pi\pi) l^- \bar{\nu}_l$  final states. The charged

multiplicity  $N_c$ , as well as the ( $\Lambda_c^+$  lepton) mass can be used to enrich the sample with respect to the elastic channel, by selecting multiplicities smaller than 2, and  $\Lambda_c^+ l^-$  masses larger than  $3.5 \text{ GeV}/c^2$ . The number of  $\Lambda_c^+$  candidates left is obtained from a fit to the mass distribution of the candidates, shown in Figure 6, and is  $62.5 \pm 10.0$ . The remaining  $\Lambda_c \pi \pi$  contribution is obtained from the simulated efficiency, after application of the enrichment selection, and is found to be  $10.0 \pm 2.8$  events. The fraction of elastic  $\Lambda_c^+ l^- \bar{\nu}_l$  events in this sample is  $r_{\Lambda_c} = 0.84 \pm 0.17$ . The  $\Lambda_c$  mass distribution of the enriched sample, together with the different components is shown in Figure 6. The slope parameter of the  $w$  distribution is determined from this enriched sample. The candidates obtained from the three decay modes of the  $\Lambda_c^+$  considered in section 4 have been separately analysed. In each of these samples, the non- $\Lambda_c^+$  background is measured from a fit to the  $\Lambda_c^+$  mass distribution.

The complementary sample, enriched in  $\Lambda_c^+ \pi \pi$ , will be used to monitor the  $w$ -shape of the  $\Lambda_c^+ \pi \pi$  background.

## 8.2 The $w$ -shape likelihood

The four-momentum of the  $\Lambda_b^0$  meson is reconstructed as described in section 6.2.2. The values of  $q^2$  and  $w$  can then be estimated. The resolutions achieved are similar to those obtained in [4], and  $\Delta w/w$  is close to  $\pm 8\%$ .

A likelihood fit to the two-dimensional  $(M(\Lambda_c), w)$  distribution is then performed, with  $2.190 < M(\Lambda_c) < 2.385 \text{ GeV}/c^2$  and  $1.0 < w < 1.6$ . The mass and  $w$  dependences are assumed to factorise in the probability distribution for each event  $k$  in channel  $i$ , where the index  $i = 1, 2, 3$  runs over the three input channels (three final states, the two lepton samples are combined):

$$P_i(M_k, w_k) = f_i^S S_i(w_k, \hat{\rho}^2) G(M_k) + f_i^{\Lambda_c \pi \pi} B_i^{\Lambda_c}(w_k) G(M_k) + f_i^B B_i^{no\Lambda_c}(w_k). \quad (21)$$

The Gaussian term  $G(M_k)$  describes the  $\Lambda_c^+$  contribution,  $B_i^{\Lambda_c}(w)$  is the inelastic background, while the combinatorial background  $B_i^{no\Lambda_c}(w)$  is mass independent in the  $\Lambda_c$  mass window investigated, as justified by a direct inspection of its shape in the simulation in Figure 6. The coefficients  $f_i^S$  (for the elastic  $\Lambda_c$  signal),  $f_i^{\Lambda_c \pi \pi}$ , and  $f_i^B$  are fixed, and are obtained from the  $pK\pi$  mass spectrum and the elastic fraction of 0.84.

In each channel  $i$ , the contribution of the signal  $S_i(w)$  is obtained from the simulated events weighted at a given  $\hat{\rho}^2$  by the squared form factor:  $\exp(-2\hat{\rho}^2(w_g - 1))$  where  $w_g$  is the generated value of  $w$ . The function  $S_i(w, \hat{\rho}^2)$  is a convolution of the physical  $w$  distribution with the detection efficiency and the resolution of the reconstruction of this variable. It has been expressed as a factorised expression, as it was easier to parametrise directly  $S_i$  rather than the resolution function:

$$S_i(w, \hat{\rho}^2) = S_i(w, \hat{\rho}^2 = 0) \exp(\hat{\rho}^2 \cdot \alpha(w)). \quad (22)$$

The function  $S_i(w, \hat{\rho}^2 = 0)$  is parametrised as  $S_i(w, \hat{\rho}^2 = 0) = a(w - 1)^m \exp(p(w - 1) + q(w - 1)^2)$ , with  $a = 0.458$ ,  $m = 0.154$ ,  $p = 17.2$ ,  $q = 40.3$ . A very good description of the simulated  $w$  distributions was obtained when the exponent  $\alpha(w)$  was assumed to be a linear function of  $w$ :

$$\alpha(w) = \alpha_0 + \alpha_1 \cdot (w - 1). \quad (23)$$

The coefficient  $\alpha_0$  is a normalisation coefficient, while  $\alpha_1$  describes the  $w$  dependence of the signal. In the absence of smearing and detector effects,  $\alpha_1$  would be -2, given the

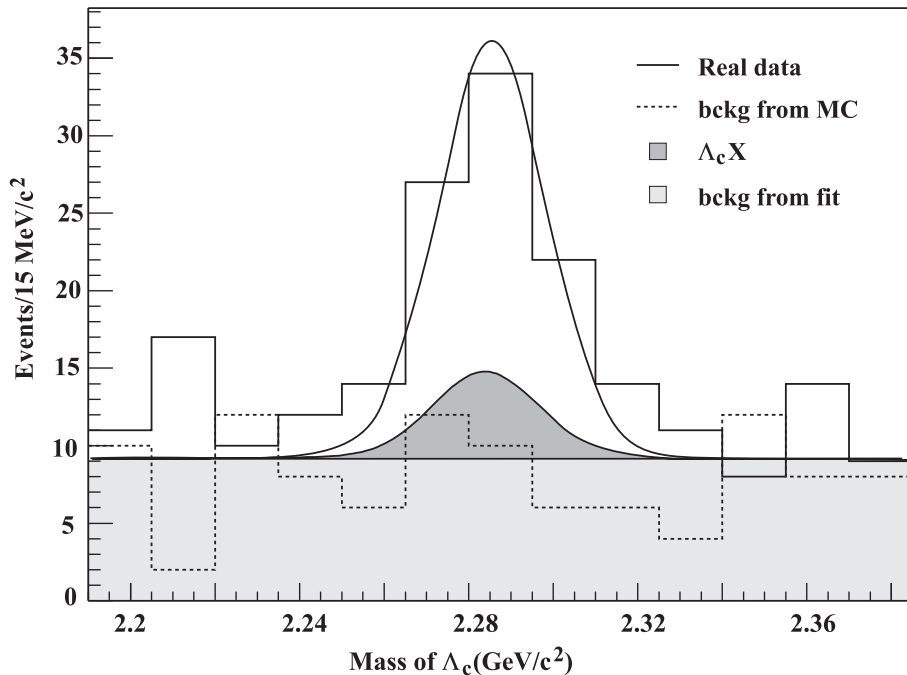


Figure 6: The  $\Lambda_c$  mass distribution in the (enriched/elastic) sample of  $\Lambda_c^+ l^-$  events used in the likelihood shape analysis (all channels). The estimated background (dotted histogram) is obtained from simulated hadronic  $Z$  decays and normalised to the actual data

exponential parametrisation in equation (7), and the actual value  $\alpha_1 = -1.67 \pm 0.08$  is close to this estimate.

The  $B_i^{\Lambda_c}(w)$  and  $B_i^{no\Lambda_c}(w)$  functions are found from the data. The shape of  $B_i^{\Lambda_c}(w)$  is obtained from the  $w$  distribution of the subsample of  $\Lambda_c^+$  events enriched in  $\Lambda_c^+ \pi \pi$ , with a charged multiplicity at the  $\Lambda_b^0$  vertex  $N_c \geq 2$  or with a  $(\Lambda_c^+ l^-)$  mass  $< 3.5 \text{ GeV}/c^2$ . A correction factor derived from the simulation is applied to the  $w$  distribution of this sample, to relate the background shapes in the enriched (elastic) and anti-enriched ( $\Lambda_c \pi \pi$ ) samples. This background, corrected for the enrichment bias is then described by a function  $B^{\Lambda_c}(w) = (w - 1)^{a_1} \exp(-b_1(w - 1))$ , with  $a_1 = 2.22 \pm 0.50$ , and  $b_1 = 27.5 \pm 5.8$ . The non- $\Lambda_c^+$  background,  $B_i^{no\Lambda_c}(w)$ , is evaluated from side-bands in the mass spectrum, chosen outside the mass window  $2.260 < M(\Lambda_c) < 2.310 \text{ GeV}/c^2$ . Its shape is described by the same parametrisation as the previous one, with new values of  $a$  and  $b$ . In the dominant  $pK^- \pi^+$  channel, for instance:  $a = 4.28 \pm 0.34$ , and  $b = 22.3 \pm 1.9$ .

The distributions of the signal in the different channels  $S_i(w, \hat{\rho}^2)$ , and the shapes of the backgrounds  $B_j(w)$  are normalised to unity, and the coefficients  $f_i^S$ ,  $f_j^B$  have been measured from the data and are fixed. The likelihood is the sum:

$\mathcal{L}_{shape} = -\sum_k \text{Log}(P(M_k, w_k))$ , and the slope obtained from the one parameter fit to the  $w$  distribution is:

$$\hat{\rho}^2 = 1.59 \pm 1.10 \text{ (stat)}. \quad (24)$$

The quality of this fit can be checked in Figure 7a, where the predicted distribution has been normalised to the observed number of events in real data. The  $\chi^2/NDF$  between the distribution predicted from the likelihood fit and the observed distributions is 5.2/11.

### 8.3 The combined event rate and $w$ shape likelihood

The information on the shape and on the absolute rate can be combined into an optimised determination of  $\hat{\rho}^2$ , assuming  $\xi_B(1) = 1$ , and a new likelihood fit is performed where the observed number of events is included as a constraint. The expected number of events  $N_{ex}$  is derived from the semileptonic branching fraction, which is itself a function of  $\hat{\rho}^2$  as described in section 7:

$$\mathcal{L} = \mathcal{L}_{shape} - N_{obs} \text{Log}(N_{ex}) + N_{ex}. \quad (25)$$

The full statistics are used for the shape likelihood, while as in section 7, the rate  $N_{ex}$  is measured only when the gas and liquid RICH are simultaneously operational, and for the  $\Lambda_c^+ \rightarrow pK^-\pi^+$  channel alone<sup>4</sup>. The actual likelihood function includes the contributions from the different backgrounds, and the value of  $\hat{\rho}^2$  obtained from this one parameter fit, shown in Figure 7b, is:

$$\hat{\rho}^2 = 2.03 \pm 0.46 \text{ (stat)}. \quad (26)$$

The statistics in Figure 7b are smaller than in 7a as only data with an operational RICH are used.

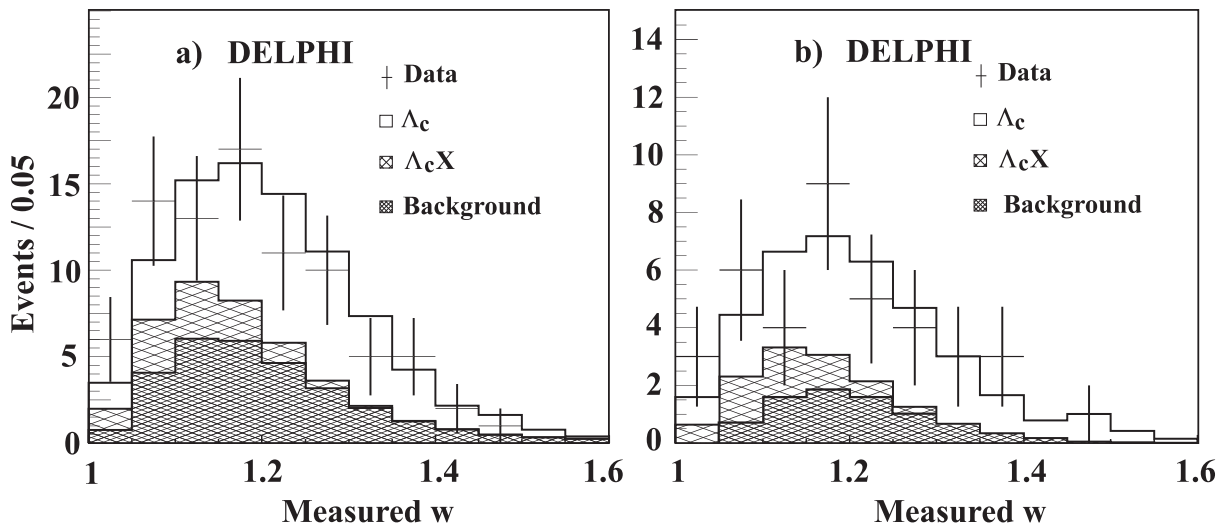


Figure 7: Comparison between fitted and measured  $w$  distributions inside the  $\Lambda_c$  mass window: a) fit to the  $w$  distribution; b) combined fit to the  $w$  distribution and the  $\Lambda_c^+ l^- \bar{\nu}_l$  rate (restricted to the working RICH sample). The statistics in Figure 7b are smaller than in 7a.

The semileptonic branching fraction corresponding to this value of  $\hat{\rho}^2$  is:

$$Br(\Lambda_b^0 \rightarrow \Lambda_c^+ l^- \bar{\nu}_l) = (5.0_{-0.8}^{+1.1} \text{ (stat)})\%. \quad (27)$$

The expected number of events is  $27_{-4}^{+7}$ , while the observed number of elastic  $\Lambda_c$  events quoted in section 7, and included in the likelihood fit, is  $27 \pm 6$ .

There are three groups of systematic errors: the errors associated to the prediction of the  $w$  shape (the identification efficiency, the parametrisation of the shape as a function

<sup>4</sup>The statistics of observed and expected events were scaled to reproduce the actual statistical uncertainty on the number of events.

source of error	$\pm$ uncertainty range	contribution to $\delta\hat{\rho}^2$
$\delta\epsilon_{id}/\epsilon_{id}$	0.15	0.08
$\delta w/w = 0.08$	0.008	0.05
$\alpha_1 = -1.67$	0.08	0.02
Fragmentation ( $\langle x_{\Lambda_b} \rangle$ )	0.008	0.05
$a, a_1$ and $b, b_1$ (shape)	stat. errors	0.01
Enriched fraction $r_{\Lambda_c} = 0.84$	0.17	0.10
Anti-enriched background shape	stat errors	0.02
$\delta B_{\Lambda_c}/B_{\Lambda_c}$ (from Table 2)	0.37	+0.70 -1.00
<b>Total</b>		+0.72 -1.00

Table 3: *Main sources of systematic uncertainties on the slope  $\hat{\rho}^2$ .*

of  $\hat{\rho}^2$ , the fragmentation), the uncertainties related to the expected yield (absolute efficiencies and branching fractions) and the systematic effects arising from the subtraction of the  $\Lambda_c$  background processes discussed in section 8.2 (parameters  $a, a_1$  and  $b, b_1$ ).

The momentum dependent uncertainties are dominated by the contribution to the global identification efficiency of the proton and kaon identification efficiencies  $\epsilon_{id}$ . The observed momentum distributions and therefore the  $w$  spectrum are sensitive to the detailed simulation of the identification algorithms. The difference between the efficiencies of proton identification in data and in simulation was monitored using a sample of selected  $\Lambda$  events. For each year, the identification efficiency as a function of momentum was measured for data and simulation. The difference typically reaches 15%. Simulated events were reweighted by the ratio of the data and simulation efficiency, and the systematic error on  $\hat{\rho}^2$  measured from the shift in  $\hat{\rho}^2$  between the original and reweighted  $w$  distributions.

The resolution on  $w$  is found to change by approximately 10% between different versions of the energy reconstruction algorithms. The impact of this uncertainty was evaluated by degrading the resolution by 10% in the simulation. Given the small contribution of the  $\Lambda_b^0$  semileptonic decays with a  $\tau$  lepton, no systematic error was assigned for this component of the signal.

The uncertainty on the number of  $\Sigma_c$  and  $\Lambda_c^*$  final states is included in the uncertainty on the fraction  $r_{\Lambda_c}$ , equal to the statistical uncertainty on its value. The systematic uncertainty on the shape of the non- $\Lambda_c$  background is evaluated by changing the shape of this background according to the statistical error on its parametrisation. This background is evaluated from the side-bands of the  $\Lambda_c$  mass spectrum.

The main systematic uncertainties on  $\hat{\rho}^2$  are summarised in Table 3, where the dominant contribution of the normalisation error (as estimated in Table 2) is singled out. The value of  $\hat{\rho}^2$  is found to be:

$$\hat{\rho}^2 = 2.03 \pm 0.46 \text{ (stat)} \quad {}^{+0.50}_{-0.60} (Br(\Lambda_c \rightarrow pK^-\pi^+)) \quad {}^{+0.50}_{-0.80} \text{ (other syst)}. \quad (28)$$

The asymmetry in the errors on  $\hat{\rho}^2$  arises from the strong non-linearity of the relation between the normalisation and the slope over the large range of  $\delta B_{\Lambda_c}$ . The contribution of the branching fraction into  $pK\pi$  to the uncertainty on the normalisation is given in Table 2, and the associated systematic error on  $\hat{\rho}^2$  has been evaluated separately in equation (28). The corresponding elastic semileptonic branching fraction is:

$$Br(\Lambda_b^0 \rightarrow \Lambda_c^+ l^- \bar{\nu}_l) = (5.0^{+1.1}_{-0.8} \text{ (stat)} \quad {}^{+1.6}_{-1.2} \text{ (syst)})\%. \quad (29)$$

To obtain  $\hat{\rho}^2$ , the prediction of HQET  $\xi(1) = 1$  has been assumed, and no theoretical uncertainty has been included in the systematic error to account for this hypothesis. A 10% change of  $\xi(1)$  would amount to a 20% change in the rate, and to 0.3 in  $\hat{\rho}^2$ .

## 9 Conclusions

A first measurement of the form factor of the  $\Lambda_b^0$  beauty baryon has been achieved in the  $\Lambda_b^0 \rightarrow \Lambda_c^+ l^- \bar{\nu}_l$  decay channel. Assuming an exponential behaviour of the Isgur-Wise function:

$$\xi_B(w) = \xi_B(1)e^{-\hat{\rho}^2(w-1)},$$

the slope parameter  $\hat{\rho}^2$  was determined from a  $w$ -shape analysis to be:  $\hat{\rho}^2 = 1.59 \pm 1.10$  (stat). If the validity of the HQET relation  $\xi(1) = 1$  is assumed, and the event rate taken into account, an improved determination of the slope can be obtained:

$$\hat{\rho}^2 = 2.03 \pm 0.46 \text{ (stat)} \stackrel{+0.50}{-0.60} (Br(\Lambda_c \rightarrow pK^- \pi^+)) \stackrel{+0.50}{-0.80} \text{ (other syst)}.$$

The evaluation of the systematic errors takes into account the actual variation of  $\hat{\rho}^2$  arising from each source.

The semileptonic branching fraction into the exclusive semileptonic mode was measured within the hypothesis  $\xi_B(1) = 1$  to be:

$$Br(\Lambda_b^0 \rightarrow \Lambda_c^+ l^- \bar{\nu}_l) = (5.0^{+1.1}_{-0.8} \text{ (stat)} \stackrel{+1.6}{-1.2} \text{ (syst)})\%.$$

The fraction of elastic  $\Lambda_c^+ l^- \bar{\nu}_l$  events is found to be:

$$\frac{\Gamma(\Lambda_b^0 \rightarrow \Lambda_c^+ l^- \bar{\nu}_l)}{\Gamma(\Lambda_b^0 \rightarrow \Lambda_c^+ l^- \bar{\nu}_l) + \Gamma(\Lambda_b^0 \rightarrow \Lambda_c^+ \pi \pi l^- \bar{\nu}_l)} = 0.47^{+0.10}_{-0.08} \text{ (stat)} \stackrel{+0.07}{-0.06} \text{ (syst)}.$$

The spectra of multiplicity, missing mass, and  $\Lambda_c^+ l^-$  mass shown in this paper strongly hint at such a sizeable fraction of non-elastic hadronic modes. This inelastic contribution is larger than assumed in the experimental determinations of the  $\Lambda_b$  lifetime, such as [29], and will affect its value, as the ratio of the  $\Lambda_c$  and  $\Lambda_b$  momenta  $p_{\Lambda_c}/p_{\Lambda_b}$  is 20% lower in the inelastic channel.

In spite of the evidence for a large inelastic contribution in semileptonic decays, no indication of charmed baryon resonances has been found in the final state.

The parameter  $\hat{\rho}^2$  reflects the structure of the  $\Lambda_b^0$  baryon. Its value is somewhat larger than in the  $b$ -meson channel, where  $\hat{\rho}^2 \sim (0.60 \text{ to } 1.3)$  as measured in [2–4]. A recent result on the  $B$  meson decays from [5] suggests an even higher value of the slope of the Isgur-Wise function for mesons, with  $\hat{\rho}^2 = 1.61 \pm 0.09$  (stat)  $\pm 0.21$  (syst). In all models proposed so far [16,18,30,31], the value of  $\hat{\rho}^2$  is expected to be larger for baryons.

## Acknowledgements

We are greatly indebted to our technical collaborators, to the members of the CERN-SL Division for the excellent performance of the LEP collider, and to the funding agencies for their support in building and operating the DELPHI detector.

We acknowledge in particular the support of

Austrian Federal Ministry of Education, Science and Culture, GZ 616.364/2-III/2a/98, FNRS-FWO, Flanders Institute to encourage scientific and technological research in the industry (IWT), Federal Office for Scientific, Technical and Cultural affairs (OSTC), Belgium,

FINEP, CNPq, CAPES, FUJB and FAPERJ, Brazil,

Czech Ministry of Industry and Trade, GA CR 202/99/1362,

Commission of the European Communities (DG XII),

Direction des Sciences de la Matière, CEA, France,

Bundesministerium für Bildung, Wissenschaft, Forschung und Technologie, Germany,

General Secretariat for Research and Technology, Greece,

National Science Foundation (NWO) and Foundation for Research on Matter (FOM),

The Netherlands,

Norwegian Research Council,

State Committee for Scientific Research, Poland, SPUB-M/CERN/PO3/DZ296/2000,

SPUB-M/CERN/PO3/DZ297/2000 and 2P03B 104 19 and 2P03B 69 23(2002-2004)

JNICT-Junta Nacional de Investigação Científica e Tecnológica, Portugal,

Vedecka grantova agentura MS SR, Slovakia, Nr. 95/5195/134,

Ministry of Science and Technology of the Republic of Slovenia,

CICYT, Spain, AEN99-0950 and AEN99-0761,

The Swedish Natural Science Research Council,

Particle Physics and Astronomy Research Council, UK,

Department of Energy, USA, DE-FG02-01ER41155,

EEC RTN contract HPRN-CT-00292-2002.

## References

- [1] P. Abreu *et al.* (DELPHI Collab.), *Zeit. Phys.* **C71** (1996) 539.
- [2] D. Buskulic *et al.* (ALEPH Collab.), *Phys. Lett.* **B395** (1997) 373.
- [3] G. Abbiendi *et al.* (OPAL Collab.), *Phys. Lett.* **B482** (2000) 15.
- [4] P. Abreu *et al.* (DELPHI Collab.), *Phys. Lett.* **B510** (2001) 55.
- [5] R.A. Briere *et al.* (CLEO Collab.), *Phys. Rev. Lett.* **89** (2002) 081803.
- [6] K. Abe *et al.* (BELLE Collab.), *Phys. Lett.* **B526** (2002) 247.
- [7] H. Georgi, B. Grinstein and M.B. Wise, *Phys. Lett.* **B252** (1990) 456.
- [8] N. Isgur and M.B. Wise, *Nucl. Phys.* **B348** (1991) 276.
- [9] H. Georgi, *Nucl. Phys.* **B348** (1991) 293.
- [10] M. Neubert, *Phys. Rep.* **245** (1994) 259.
- [11] K.C. Bowler *et al.* (UKQCD Collab.), *Phys. Rev.* **D52** (1995) 5067.
- [12] E. Bagan, P. Ball and P. Gosdzinsky, *Phys. Lett.* **B301** (1993) 249;  
 B. Blok and M. Shifman, *Phys. Rev.* **D47** (1993) 2949;  
 M. Neubert, *Phys. Rev.* **D47** (1993) 4063;  
 S. Narison, *Phys. Lett.* **B325** (1994) 197.
- [13] B. Holdom, M. Sutherland and J. Mureika, *Phys. Rev.* **D49** (1994) 2359.
- [14] I. Caprini, L. Lellouch and M. Neubert, *Nucl. Phys.* **B530** (1998) 153.
- [15] C.G. Boyd, B. Grinstein and R.F. Lebed, *Phys. Rev.* **D56** (1997) 6895.
- [16] D. Chakraverty *et al.*, *Int. J. Mod. Phys.* **A14** (1999) 2385.
- [17] B. Holdom and M. Sutherland, *Phys. Rev.* **D47** (1993) 5067.
- [18] M. Sadzikowski and K. Zalewski, *Z. Phys.* **C59** (1993) 677.
- [19] M. E. Luke, *Phys. Lett.* **B252** (1990) 447.
- [20] M. V. Manohar and M. B. Wise, *Heavy Quark Physics*, Cambridge University Press (2000), Cambridge (U. K.).
- [21] P. Aarnio *et al.* (DELPHI Collab.), *Nucl. Instr. & Meth.* **A303** (1991) 233.
- [22] P. Abreu *et al.* (DELPHI Collab.), *Nucl. Instr. & Meth.* **A378** (1996) 57.
- [23] V. Chabaud *et al.*, *Nucl. Instr. & Meth.* **A368** (1996) 314.
- [24] T. Sjöstrand, *Comp. Phys. Comm.* **39** (1986) 347;  
 T. Sjöstrand and M. Bengtsson, *Comp. Phys. Comm.* **43** (1987) 367;  
 T. Sjöstrand, *JETSET 7.3 manual*, CERN-TH 6488/92(1992).
- [25] K. Hagiwara *et al.* (Particle Data Group), *Phys. Rev.* **D66** (2002) 010001.
- [26] P. Abreu *et al.* (DELPHI Collab.), *Zeit. Phys.* **C57** (1993) 181.
- [27] G. Bonvicini *et al.* (CLEO Collab.), *Phys. Rev.* **D57** (1998) 6604.
- [28] T. Sjöstrand, *Comp. Phys. Comm.* **82** (1994) 74.
- [29] P. Abreu *et al.* (DELPHI Collab.), *Eur. Phys. J.* **C10** (1999) 185.
- [30] F. Cardarelli and S. Simula, *Phys. Lett.* **B421** (1998) 295.
- [31] Y.B. Dai, C.S. Huang, M.Q. Huang and C. Liu, *Phys. Lett.* **B387** (1996) 379;  
 E. Jenkins, A. Manohar and M.B. Wise, *Nucl. Phys.* **B396** (1993) 38.